UNIVERSITY OF PADOVA

Department of
Agronomy, Food, Natural resources, Animals and Environment

Second Cycle Degree (MSc) in
Food Science and Technology

Sucrose stearate as food-grade stabilizer for lipid-based nanoparticles: characterization of the internal structure and time stability of eicosapentaenoic acid loaded mesosomes

Supervisor:
Prof. Andrea Curioni

Assistant supervisor:
Prof. Michael Rappolt
Dott. Arwen Tyler

Student:
Filippo Ceola

Student number:
1131436

ACADEMIC YEAR
2016 – 2017

To my sister Erica, for being an example

of strength and perseverance.

Contents

I. Abstract

Lyotropic liquid crystalline mesophases of monoglycerides are widely used to design drug delivery systems. In the present work, the lipid matrix was composed mainly of monolinolein and monoolein, and eicosapentaenoic acid (EPA) was used as guest molecule. Sucrose stearate was investigated as a new food-grade stabilizer. Firstly, phase diagram of the EPA/monoglycerides system in excess water was completed; secondly, the most interesting EPA-loaded samples were dispersed with two different surfactants. The largely used and well-known Pluronic® F127 and the food-grade sucrose stearate are compared in terms of stabilization effectiveness; effect on internal structure, particle size and time stability have been investigated in detail.

Although sucrose stearate appears not to be as good as Pluronic® F127, it induces *Im3m* structure swelling, which allows to eventually load larger compounds, and it has a stability in the range of 9 – 15 days, depending on the EPA load. Even though sucrose stearate stabilized nanoparticles can be only used for fresh products with limited shelf life at the moment, more research should be done in this direction, because such innovative delivery vehicles have already shown great potential in the pharmaceutical field and appear to be very promising in the food area, as well.

II. Riassunto

Le strutture mesofasiche dei cristalli liquidi liotropici a base di monogliceridi sono ampiamente utilizzate per veicolare farmaci. In questo lavoro, la matrice lipidica era composta prevalentemente di monolinoleina e monooleina, mentre l'acido eicosapentaenoico (EPA) è stato utilizzato come molecola ospite. Il saccarosio stearato è stato testato come stabilizzante *food-grade,* per l'applicazione in campo alimentare. Per prima cosa è stato realizzato il diagramma di fase del sistema monogliceridi/EPA in eccesso di acqua e, successivamente, i campioni più interessanti sono stati dispersi utilizzando due diversi stabilizzanti. Il molto usato e ben conosciuto Pluronic F127 e il saccarosio stearato, candidato per l'industria alimentare, sono stati confrontati in termini di efficienza di stabilizzazione; la struttura interna e la stabilità nel tempo delle dispersioni sono state analizzate a tal proposito.

Sebbene il saccarosio stearato non risulti essere performante tanto quanto il Pluronic F127, esso induce il rigonfiamento della struttura *Im3m* consentendo quindi l'eventuale inserimento di molecole più grandi ed, inoltre, garantisce 9 - 15 giorni di stabilità, a seconda della quantità di EPA. Ciò significa che, ad oggi, l'impiego di nanoparticelle stabilizzate con saccarosio stearato è limitato a prodotti freschi con breve shelf-life, ma più ricerca dovrebbe essere condotta in questa direzione perché il potenziale di questi *carrier* innovativi sta già dimostrando grande potenziale in ambito farmaceutico e sembra essere molto promettente anche in campo alimentare.

III. Acknowledgments

I would like to thank Professor Andrea Curioni, for all your help with the organization of the research period abroad and your support with many aspects of this project.

I express my sincere gratitude to Professor Michael Rappolt for taking me in, in the School of Food Science and Nutrition (Leeds, UK). Thank you for the many discussions, scientific and not, and for your great assistance with this project.

Thanks to Doctor Arwen Tyler for your very important help during the laboratory work and for taking me to your beamtime at the synchrotron. Your enthusiasm and interest in this work have been stimulating and inspiring.

I thank Diamond Light Source for access to beamline I22 that contributed to the results presented here.

To my family, and especially my parents, thank you for your support, encouragement, making sure I was always well fed and for your unconditional love. Your hard work and sacrifices during all these years have given me the opportunity to study, travel and do many other experiences. For all this, I will always be grateful.

Finally, thanks to my dearest friends! You have been part of my life for so many years that I cannot think of a life without any of you.

IV. Abbreviations

ALA	α-linolenic acid
CPP	critical packing parameter
DHA	docosahexaenoic acid
DLS	dynamic light scattering
DU	Dimodan® U
EME	emulsified micro-emulsion
EPA	eicosapentaenoic acid
FA	fatty acid
GI	gastro-intestinal
LBP	lipopolysaccharide binding proteins
LCFA	long-chain fatty acid
ML	monolinolein
MO	monoolein
NaCas	sodium caseinate
PdI	polydispersity index
PUFA	polyunsaturated fatty acid
rTG	re-esterified triglyceride
SAXS	small angle X-rays scattering
SDD	sample-to-detector distance
SSL	sodium stearoyl lactylate
TG	triglyceride
UWL	unstirred water layer
WPI	whey protein isolate

1 Introduction

1.1 Biological lipid classes and lipid self-assembly

Biological lipids have been classified by Small in 1968, as shown in **Figure 1.1**. Depending on their physical properties and interactions in bulk aqueous system, as well as at the air-water or oil-water interface, lipids were organized in two classes: non-polar and polar lipids. The latter are divided in three subclasses, based on the self-assembly behavior.

Looking at polar lipids, in class I there are insoluble, non-swelling amphiphiles. Di- and triglycerides, long-chain protonated fatty acids and alcohols, waxes, sterol esters, phytols, retinols, fat-soluble vitamins and cholesterol belong to this group.

Polar lipids in class II are insoluble, with swelling properties. Molecules as lecithin, monoglycerides and fatty acids self-assemble to form well-defined structures in bulk liquids (e.g. water or intestinal fluids).

Soluble amphiphiles belong to class III, they have clear polarity between the hydrophobic and hydrophilic moieties and organize in self-assembled phases when in contact with water. This class is further subdivided into anionic, cationic, non-ionic detergents and lyso-lecithin in one group, and into bile salts, saponins, rosin soaps and phenanthrene sulfonic acids in the other [1].

In the context of this work, monoglycerides self-assembly properties are the most significative. Monoglycerides possess both hydrophobic and hydrophilic moieties, the water-soluble part is generally called the “head”, while the water insoluble one is recognized as the “tail”. The self-assembly process can be manly attributed to the hydrophobic effect: water soluble moieties shield the non-polar regions from water molecules, by aggregating in thermodynamically stable structures [2].

These particular phases have optical, physical and structural properties in between the two classic crystalline solid and isotropic liquid states. Not a single transition from solid to liquid is present, but rather a series of transitions from the one to the other. Thus, liquid crystal mesophases describe a state of matter that shows both solid and fluid-like

characteristics. In particular, if their self-assembly properties are tunable by changing pH or solvent composition, they are called lyotropic liquid crystals (LLCs), whereas thermotropic liquid crystals are rod- or disc-shaped structures that form in a certain temperature range [2]. Biological lipids show lyotropic characteristics.

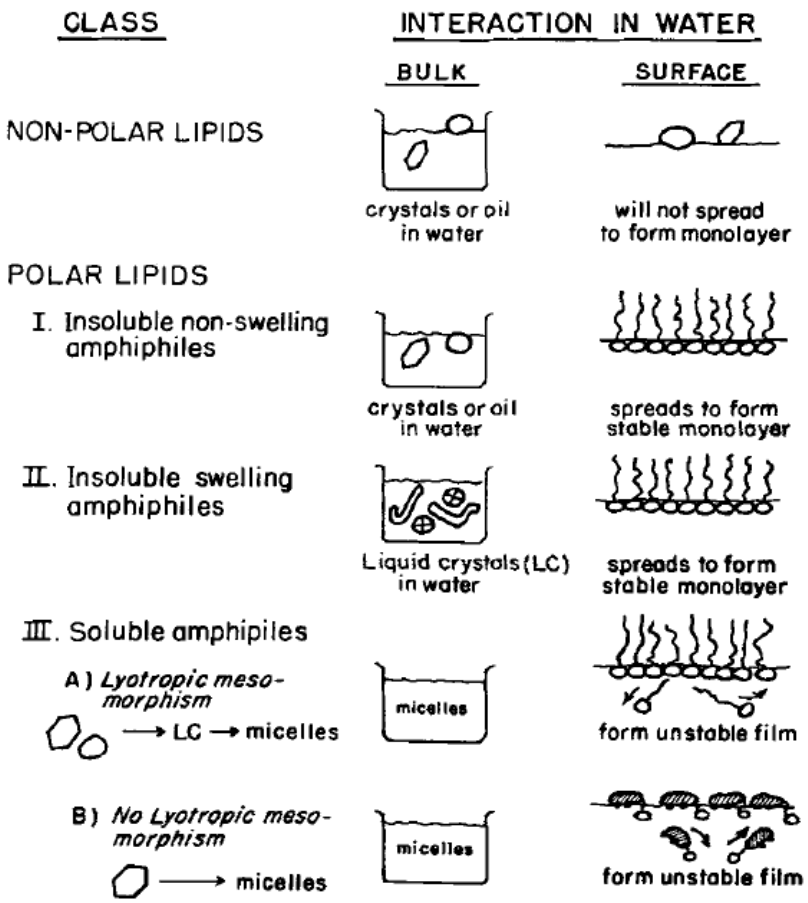

Figure 1.1. Biological lipids classification. Figure reproduced from [1].

1.2 Driving forces for liquid crystals formation

Fully understanding the structuring behavior of lipids self-assembled liquid crystalline phases would require the detailed study of lipid-lipid, lipid-oil, lipid-water and lipid-oil-water interactions. These structures are affected by molecular characteristics such as number of double-bonds in the alkyl chain, type of double-bonds, length of the hydrophobic chain, size and configuration of the "head" group and eventually the presence of hydrophobic or hydrophilic additives. In addition, temperature, pressure,

solvent, electrostatic interactions, hydration level and other possible experimental conditions need to be considered [3].

A good qualitative understanding of the aggregation behavior of amphiphilic molecules can be obtained with the support of the *critical packing parameter* (CPP), a dimensionless number which allows to foresee the type of aggregation. It is defined as following:

$$CPP = \frac{v_s}{a_0.l} \quad (1)$$

where v_s is the hydrophobic chain volume, a_0 is the head group area and l is the hydrophobic chain length. It represents the ratio between the effective volume of the alkyl chain and the volume of a theoretical cylinder having the base area equal to the head group surface and the height as long as the alkyl chain. The value the CPP of a mono- or di-glyceride indicates if the aggregation is more likely to lead to normal (type 1) or inverse phase (type 2). In terms of emulsions, the normal phase is an oil-in-water emulsion, whereas the water-in-oil emulsion is conventionally addressed as the inverse phase. If CPP < 1, molecules have a cone shape and assembly with a positive convex curvature leading to an oil-in-water emulsion, while for CPP > 1 the wedge shape induces negative curvatures, thus a concave structure where the hydrophobic chains stretch towards the apolar region and the polar heads shield the hydrophobic moieties of the lipophilic region, preventing them to come in contact with water. When CPP = 1, molecules are cylinder-like shaped and the mean curvature of the related structure is zero, thus they self-assemble in a planar structure **Figure 1.2** [4, 5, 6].

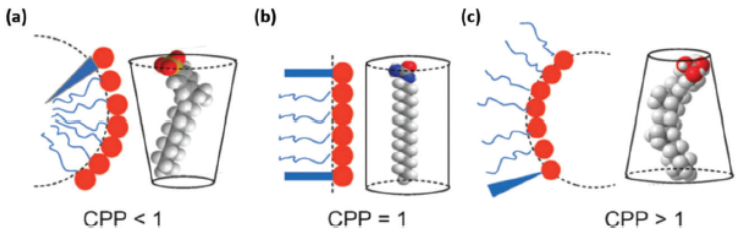

Figure 1.2. a) the critical packing parameter (CPP) is < 1 thus the curvature is positive and an oil-in-water emulsion forms; b) for CPP = 1 the curvature is zero, a planar layer forms; c) when CPP > 1 the molecules are wedge shaped and self-assemble in a reverse structure. Figure reproduced from [3].

The second driver that determines the configuration of amphiphiles in mesophases is the *packing frustration.* This concept can be interpreted as the optimization of packing of elements in a uniform geometry. **Figure 1.3** shows, for example, a section of cylinders into hexagonally close packed system. Such structure generates 9% void space which represents an unsustainable situation from an energy point of view. In order to overcome that energy penalty, alkyl chains of amphiphilic molecules stretch towards the apolar region, away from their preferred conformation. Beyond the stretching limit, phase transition occurs to a more sustainable configuration. The stretching ability is influenced by the temperature. Higher values enhance the mobility of alkyl chains and thus accelerate phase transition [3].

There are also other factors influencing mesophases configuration and transition, like lateral pressure, interfacial curvature, curvature elasticity, but their in-depth analysis is out of the scope of this work.

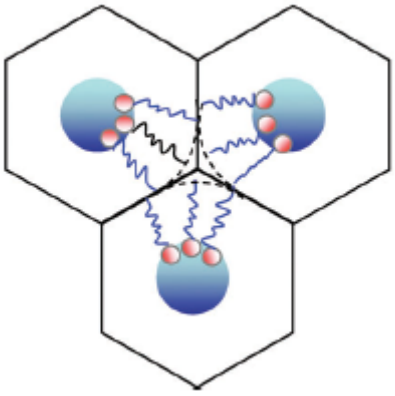

Figure 1.3. Section of cylindrical shapes packed into hexagonal configuration. Amphiphiles' hydrophobic chains stretch towards the void space away from their preferred conformation, to relief the packing frustration. Figure reproduced from [3].

1.3 Mesophases characterization

Most common amphiphiles self-assemble into 1, 2 and 3 dimensional structures in the presence of water: lamellar, hexagonal and cubic, respectively. Depending on the aforementioned driving forces and the amount of water present in the system, they

assembly into normal or inverse phases. **Figure 1.4** shows the different nanostructures that occur at different values of CPP and water content.

The reverse phase has been acknowledged particular interest because peculiar mesophases appear in excess of water and are of much interest as potential delivery vehicles for food bioactives and drugs, in particular for the ability of solubilizing poorly water-soluble components, with a positive effect on their bioavailability. Type 2 structures includes inverse bicontinuous cubic phases, inverse hexagonal phase, inverse cubic micellar and inverse micelles [6, 7, 8].

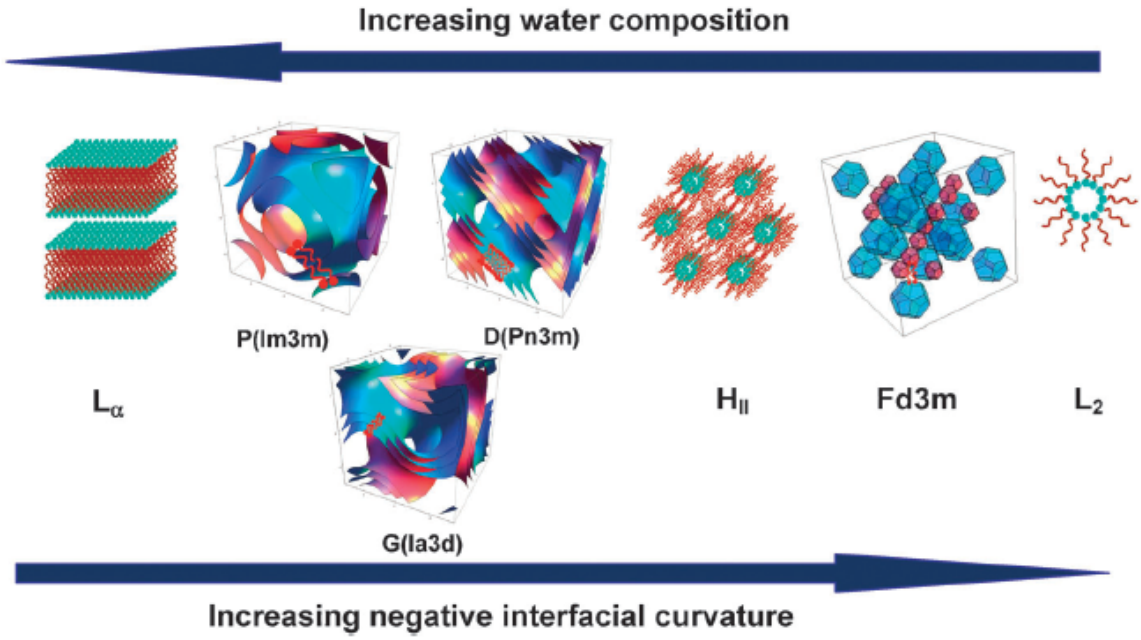

Figure 1.4. Representation of type 2 (inverse) structure and their variation as water content or critical packing parameter (CPP) change. L-R: L_α lamellar phase, P-D-G bicontinuous cubic phases, H_2 hexagonal phase, Fd3m cubic micellar phase and L_2 inverse micelles. Figure reproduced from [3].

1.3.1 Lamellar phase

The lamellar phase consists of a stack of amphiphilic bilayers separated by water layers. Each bilayer involves amphiphilic molecules which hydrophobic tails face each other and polar heads are in contact with the water molecules that are located between the bilayers. Ideally, the lateral repulsive pressure among adjacent hydrocarbon chains is well counterbalanced by the interfacial pressure, giving rise to a structure with zero

mean curvature. As they do not possess any curvature towards the water nor the alkyl chains regions, they evolve in 1-dimensional repetitive flat layers (1D-stacking). In Small Angle X-ray Scattering (SAXS) observations they are evidenced by peaks apparent at scattering angles following the ratios of 1: 2: 3: 4… . Among a large variety of lamellar phases, the L_α phase nominates the fluid liquid crystalline one. Due to the fluidity and mobility of the amphiphilic molecule across the layer, it is the biologically most relevant lamellar phase [5, 6].

1.3.2 Inverse bicontinuous cubic phases

The clever addition of other compounds such as fatty acids to L_α phase can trigger the transition to inverse lyotropic phases, either by (i) increasing the negative interfacial curvature modulus and/or by (ii) by decreasing of packing frustration in the lamellar structure. This, for instance, can lead to the formation of bicontinuous cubic phases, as shown in **Figure 1.4**. They are so-called bicontinuous cubic phases, because they are organized in a 3-dimensional bilayer structure separating two interpenetrating but non-communicating water channel networks with periodic minimal surfaces, in order to reach the most favorable thermodynamic state. Inverse bicontinuous cubic mesophases are conventionally identified by the symbols V_2 or Q_2 and exist three different crystallographic configurations.

The most common space groups are called *Im3m, Pn3m* and *Ia3d*, based on geometric symmetry. *Im3m* is based on the Schwartz primitive (P) minimal surface. Its unit cell has three mutually perpendicular water channels which are arranged in a cubic 3D-lattice. The so-called diamond structure (D) has crystallographic space group *Pn3m*, it is also constituted by two non-communicating water channels shielded by a bilayer but in this structure each unit is formed by aqueous channels that meet at a tetrahedral angle of 109.5° and form a diamond lattice. *Ia3d* crystallographic symmetry is based on the Schoen gyroid (G) minimal surface. The structure is made of two independent water channels separated by a bilayer, but in this case the aqueous channels are interpenetrating left-handed and right-handed helices.

Water channel diameters can range from 4 to 20 nm based on the type of space grouping and hydration level. The most hydrated structure is the primitive (P) *Im3m*, followed by the diamond (D) *Pn3m* and finally by the gyroid (G) *Ia3d.* In SAXS patterns

they are evidenced by peaks in ratios of √2: √4: √6: √8: √10: √12…, √2: √3: √4: √6: √8: √9... and √6: √8: √14: √16: √20…, respectively [4, 6, 7, 9].

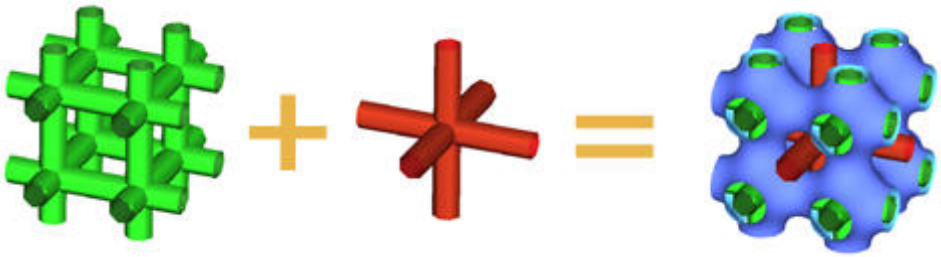

Figure 1.5. Representation of the two interpenetrating non-communicating aqueous channels in the primitive configuration *Im3m.* Figure taken from [10].

1.3.3 Inverse hexagonal phase

H_2 phase ideally consists of practically infinite long rod-shaped lipid monolayers, which aggregate on a 2-dimensional hexagonal lattice, as shown in **Figure 1.4**. In the inverse phase the surface has negative curvature towards the aqueous internal phase. When analyzed in SAXS, H_2 phase shows peaks in the ratio of 1: √2: √4… [5].

1.3.4 Inverse cubic micellar phases

Usually identified with I_2, they have been proposed to consist of arrangements of two different-sized micellar structures on a periodic lattice, e.g. *Fd3m* is composed by micelles in a double diamond arrangement, as represented in **Figure 1.4**. This phase occurs only in particular systems of lipids and water and at narrow range of temperature. *Fd3m* shows peaks in the ratio of √3: √8: √11: √12: √16: √19… in SAXS analysis [5, 9].

1.3.5 Inverse micellar phase

The so-called L_2 phase is a water-in-oil microemulsion containing inverse micelles. It forms at a very low water content or high temperature. In SAXS it is not identified by various peaks; the highest intensity at the scattering vector q_{max} indicates the positon of the first form factor maximum instead, which is related to the next nearest neighbor distances of the inverse micelles [6].

1.4 Self-assembly monoglycerides and guest molecules

1.4.1 Monoolein and monolinolein

Among amphiphiles, monoglycerides such as glycerol monooleate, also known as monoolein (MO), and glycerol linoleate, or monolinolein (ML), have been largely studied as self-assembly lipids for nanocarriers formulation. They consist of a polar glycerol backbone which is bonded to an alkyl chain, with single or double unsaturation, respectively. Monoolein carbon chain has a *cis* double-bond in position 9, whereas monolinolein carbon chain exhibits one cis double-bond in position 9 and the second one in position 12. The presence of *cis* double-bonds is extremely important for the self-assembly of lipid mesophases because it affects the alkyl chain splay and thus the critical packing parameter (CPP), **Figure 1.6**.

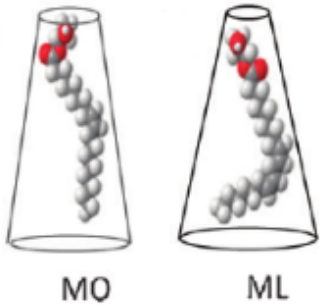

Figure 1.6. L-R, MO (monoolein) and ML (monolinolein) structures affect hydrocarbon chain splay, thus the critical packing parameter (CPP) and they self-assembly properties. Figure adapted from [5].

Figure 1.7 shows the phase diagrams of MO and ML at different temperatures, as function of the water content. Despite of what was aforementioned about the phase transition sequence at increasing water content, it is worth to notice that L_α is present at very low water content. Such peculiar behavior cannot be explained using the CCP principle. What happens is that there is not sufficient free water to fill the water channels of the cubic phases. All the water molecules are bonded to the hydrophilic headgroup and distribute on the planar membranes of the lamellar phase. The L_α phase must be considered highly curvature-frustrated because of this constraint and it also explains the fast conversion from fluid lamellar bilayer to the crystalline structure L_c. The L_c phase has not been mentioned before; it consists of a lamellar bilayer in which

molecules have no freedom of mobility due to the reduction in the effective alkyl chains volume (v_s)[6].

Above a certain water content (35-50% depending on the monoglyceride) phase separation occur into a structured water-containing oil phase and a water-excess phase. That indicates the maximum solubilization capacity for water within the lipid structure; the bicontinuous cubic phases have the best capacity of solubilizing water, followed by the hexagonal, cubic micellar and inverse micellar phases [5].

In **Figure 1.7** it is possible to notice that only some of the aforementioned mesophases show up in the monoolein/water and monolinolein/water systems.

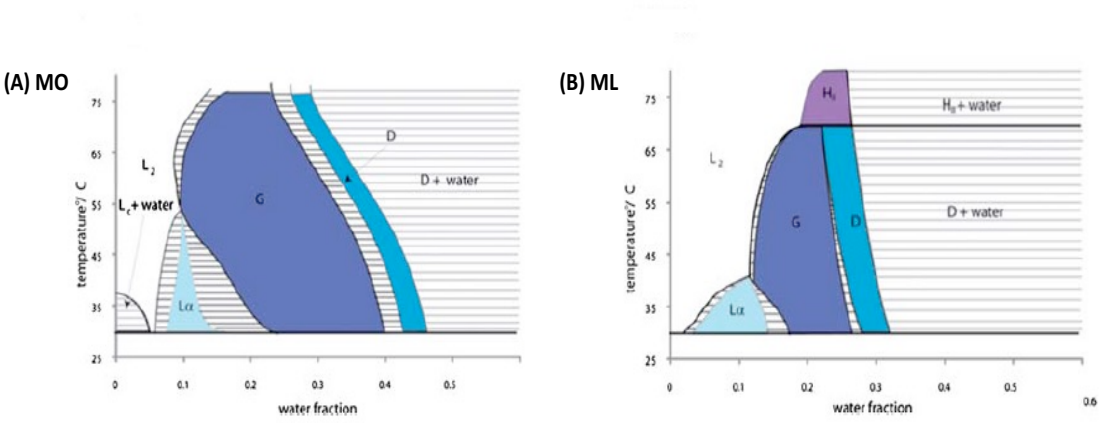

Figure 1.7. Water content – temperature phase diagrams of (A) monoolein and (B) monolinolein. The symbols: (L_α) fluid lamellar, (P) primitive cubic, (D) diamond cubic, (G) gyroid cubic, (H_2) hexagonal, (L_2) inverse micellar. Figure taken from [11].

1.4.2 Guest molecules and temperature influence on phase transition

Self-assembled mesophases consist of two domains, one hydrophobic and one hydrophilic, which are separated by an amphiphilic layer. Such conformation contains an extremely large surface (about 400 m^2/g in the case of bicontinuous phases [8]) that can be used to incorporate guest molecules in order to create delivery vehicles or tune phase assembly. In fact, lyotropic liquid crystals can be tuned by modification of solvent or additives content. Guest compounds can be hydrophilic, amphiphilic or hydrophobic. Depending on the nature, they can be positioned within the water network (water-soluble compounds), in the apolar domain if lipophilic or at the interface in case of amphiphilic guest molecules [5, 7].

Guest molecules deeply influence the phase behaviour of the binary monoglyceride-water system. Lipophilic molecules induce a more negative mean curvature, thus transitions occur in the sequence: V_2 → H_2 → Fd3m → L_2. This is understood, since apolar guest molecules reduce the packing frustration, in other terms filling the "voids" of the self-assembled structures. In addition, lipophilic compounds lead to what can be seen as both a significant reduction in water up-take and water expulsion from the aqueous channels, therefore as strong contribution towards more negative curvature phases [6].

Hydrophilic molecules show two different behaviors, they can be either kosmotropic or chaotropic solutes. The first ones interfere with the water molecules network resulting in dehydration of the headgroups and consequently in a more negative mean curvature of the lipid/water interface. This situation occurs when the hydrophilic compound is a strong hydrogen bond acceptor, thus the number of water molecules binding the monoglyceride polar head is reduced. Alternatively, chaotropes lead to an increase of the mean curvature because they tend to destabilize water structure. Hence, they induce the formation of L_α phase from the hexagonal and cubic phases [7, 12].

In this work, the inclusion of omega-3 fatty acids is investigated. Due to their hydrophobic nature and the high degree of unsaturation, omega-3 fatty acids is expected to induce the formation of highly negative mean curvature surfaces. Ternary system of monoglycerides/fish-oil/water well represent this behavior. In this study, Dimodan® U (DU), manufactured by Danisco Co Ltd. (Denmark), was used as monoglyceride mixture, which is mainly composed of monolinolein and monoolein. As representative of fish oil, eicosapentaenoic acid (EPA) by Cayman Chemical Company (USA) was included [13]. A shift from the bicontinuous cubic to hexagonal and, finally, inverse micellar phase can be noticed as the guest compound (EPA) content is increased.

In addition, temperature influence on the phase behavior has to be taken into account. When temperature increases, the alkyl chains splay increases, i.e. v_s increases, and consequently the polar heads get dehydrated, leading to a reduction in the effective occupied area. These factors lead to a relief of packing frustration as well as to a more

convex curvature of the amphiphilic layers. Therefore, increasing the temperature also promotes phase transition in the order of $V_2 \rightarrow H_2 \rightarrow Fd3m \rightarrow L_2$.

1.5 Mesophases: dispersion, application and stabilization

1.5.1 Mesosomes and their application

Bulk liquid crystal systems are thermodynamically stable systems when swollen with water. In presence of a stabilizer, they can be dispersed in submicron particles of few hundred nanometres size which internal structure can change due to interaction with the stabilizer. Cubic, hexagonal, micellar cubic and inverse micellar dispersed phases are named cubosomes, hexosomes, micellar cubosomes and emulsified micro emulsions (EMEs), respectively; in general, they have been recently addressed as *mesosomes* or ISA*somes*, as the particles envelope *Internally Self-Assembled* structures [6, 14, 15].

Mesosomes represent a delivery vehicle for many different compounds, either hydrophilic, hydrophobic or amphiphilic. Due to the large surface area of the internal phase, they offer an excellent loading and delivery capacity and highly increase solubility of poorly water-soluble compounds. In fact, it has been calculated that if the same volume of cubic phase is considered, the surface area of cubosomes with 200nm diameter is 200'000 times larger than for the bulk phase [8]. Moreover, self-assembled liquid crystalline phases show 10-20 times more solubility capacity than that of any other water or oil phase [16].

Lots of different application have been explored and will be eventually further investigated. Mesosomes are largely studied for enhanced solubilisation and sustained release of drugs, nutrients and aromas, control of membrane crystallization, improved bioavailability and delivery of bioactive compounds, ingredients protection from oxidation and formulation of biosensors and chemical reactors [17, 18]. The latter is widely reported in the field of green and organic chemistry. EMEs stabilized by Span 80 are used as location for synthesis of nanoparticles, for example for lithium batteries [19].

Mesosomes as chemical reactors is becoming very interesting in food field as well; their suitability for hosting chemical reactions is mainly attributed to three reasons: firstly, a large variety of molecules with different hydrophobicity can be solubilized in one single phase; secondly, partitioning and concentration of reagents and products increase the specific reaction rate; thirdly, internal surface structure of the lyotropic phase can influence reaction regioselectivity, due to the orientation of the molecules at the interface [16]. Synthesis of Maillard reaction products has been used to investigate the effectiveness and efficiency of mesosomes as reactors. One example is the production of norfuraneol from two different precursor systems: xylose/glycine and xylose/leucine. The reaction was carried out at 70°C in different mesophases obtained from mixtures of 80% saturated and unsaturated monoglycerides and 20% water. After 7 hours of incubation, a 1.7- and 3-fold increase in norfuraneol level was detected in hexosomes using xylose/glycine and xylose/leucine, respectively, compared with the use of an aqueous media [20]. Another example shows the different performance between reverse micelles and reverse bicontinuous cubic phase. The first was prepared using 80% unsaturated MG (Dimodan® U) and 20% water, the latter using 80% saturated monoglycerides (Dimodan® HR) and 20% water. The formation of 2-furfurylthiol from L-cysteine and furfural was induced at 100°C and resulted 5 times higher in reverse micelles and 7 times higher, than in an aqueous phase [21].

In terms of compounds bioavailability, there are several studies reporting facilitated uptake especially of lipophilic molecules. In-vitro experiments show that the high solubilisation capacity of a lipid-based formulation prevents hydrophobic compounds from precipitation in the gastro-intestinal (GI) tract, therefore a significant improvement in in-vivo bioavailability is expected when compared to a non-solubilized suspension formulation. For example, an in-vitro study was conducted to assess the bioavailability of a lipophilic drug (atovaquone). Different types of lipid-base formulations have been investigated showing a 3.5-fold increase in atovaquone bioavailability compared with the aqueous suspension [22].

Another interesting application exploits the facts that lyotropic liquid crystalline phases appear during natural emulsification and digestion of lipids in the GI tract, as will be better explained in the next sessions. Mimicking those structures allows to deliver

vitamin E to patients with chronic pancreas insufficiency. Vitamin E (tocopherols and tocotrienols) are powerful anti-oxidants which act as radical scavenging preventing chain propagation of lipid oxidation. Vitamin E is also related to lowered risk of coronary heart disease and atherosclerosis. People with pancreas insufficiency suffer from inadequate production of digestive enzymes, inefficient enzymes activation or disturbed enzymes deactivation. This condition often leads to general maldigestion and malabsorption, with consequent vitamin deficiency (in particular of vitamins A, D, E and K). Formulation of free and acetylated α-tocopherol solubilized in dispersed cubosomes and micelles was delivered directly to the small intestine of patients by tube-feeding and blood level of d6-α-tocopherol and d3-α-tocopheryl was calculated. No difference was detected between the bioavailability of free and acetylated α-tocopherol, using either dispersed bicontinuous cubic phase or micellar formulations. Moreover, absorption of vitamin E from cubosomes and micelles resulted higher than that from a standard breakfast but lower than that of fortified cereals, probably because they slow down the transit of food in the intestine hereby prolonging the time available for absorption. However, these findings show promising application of self-assembled lipid nanostructures for treating patients under malabsorption conditions or with no options for solid food intake [23].

These are just few of the several possible applications which have been explored, other examples present in literature are i) oral bioavailability in rats of the poorly water soluble drug *cinnarizine* in a lipid-based liquid crystalline matrix [24], ii) pH-responsive mesosomes designed to trigger compound release in response of pH changes between stomach and intestinal environment [25], iii) phosphatidylcholine (SPC)/glycerol dioleate (GDO) formulation which incorporates significantly high amounts of antioxidant quercetin which can be delivered both as bulk phase formulation and dispersion [26].

One of the major bottlenecks that has prevented the exploitation of these particles for certain application is the incapacity to control and tune highly swollen structures. The water cannels[1] of the bicontinuous cubic phase have usually 4 nm wide diameter which

[1] The lattice parameter of such liquid crystalline structure is the distance between two water channels centres, which can be also seen as the sum of the thickness of the bilayer and the diameter of a water

precludes the possibility to load molecules larger than that. Lots of research has been conducted to design particles with water channels 30 – 40 nm wide which were only found in nature as transient structure, until recent times. One solution to induce swelling is to dope the structure with hydration-modulating surfactants such as sucrose stearate or poly-glycerol ester. Sun et al. obtained a bicontinuous cubic phase Pn3m with water channels of 7.2 nm diameter instead of 3.5 nm, when introducing sucrose stearate, due to enhanced hydration at equilibrium from 35 % to 52% water content within the structure [27]. In 2015, Tyler et al. managed to reach a water channel diameter of 24.9 nm and a total lattice parameter of 47 nm by adding cholesterol to make the bilayer stiffer and introducing anionic lipids to induce electrostatic repulsion across the water channels [28].

Even though a few products based on lipid nanoparticles are already available, further research is necessary for better understand the interactions between the various components of such system. This will allow to tune particles' properties and design very specific structure for different purposes.

channel. The **water channel radius** can be easily calculated by using equations (10) and (11) in section 3.1.2.

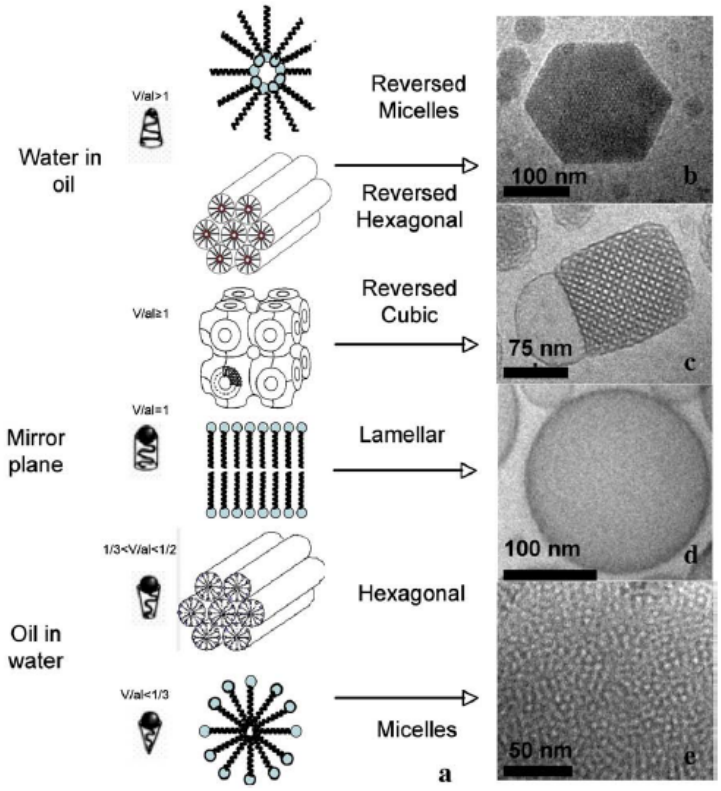

Figure 1.8. On the left, Cryo-TEM images of different mesosomes and their correspondent self-assembly structures and critical packing parameter (CPP). Images (from the top to the bottom) show a hexosome, a cubosome with primitive internal structure, a vesicle with lamellar structure and finally a dispersed micellar phase. Reproduced from [29].

1.5.2 Mesosomes stabilization

As stated before, mesosomes are submicron sized particles obtained from the dispersion of fully hydrated lyotropic liquid crystalline mesophases. In order to prevent particles destabilization and coalescence, an emulsifier needs to be added to the mixture. In many studies, Pluronic® F127 (MW of approximately 12600 g/mol) has been used. It is a synthetic triblock copolymer which consists of one poly(propylene oxide) block (PPO) between two poly(ethylene oxide) blocks (PEO). Copolymer F127 absorbs at the oil-water interface of particles building a corona that sterically stabilize the dispersion. In particular, its hydrophobic moiety (PPO) is in contact with the oil phase, whereas the hydrophilic ones (PEO) point to the water phase [30].

Stabilizers may interact with the internal structure of mesosomes. Thus, selection of the appropriate emulsifier plays a key role in the formation and stability of particles. It is

recognized that steric stabilization has little impact on the mesophase nature compared with electrostatic one. Charged emulsifiers show high propensity to disrupt the internal phase and they have also been reported to lead to toxic carriers [4].

Modification in the internal phase of cubosomes, hexosomes and EMEs has been studied in relation to triblock copolymer F127 concentration showing different behaviour based on the liquid crystalline phase. In case of cubosomes the study was conducted on a system of pure ML, with no guest molecules added. Phase transition was observed, from the bicontinuous cubic phase *Pn3m* to *Im3m* when increasing the emulsifier content. Defined β as $\frac{\text{mass of emulsifier}}{\text{mass od lipid+mass of oil}} \text{x}100$, at β=2 the crystallographic configuration *Pn3m* was detected in SAXS analysis, whereas for values within the range 4 to 8 *Pn3m* phase coexisted with *Im3m* and for β values from 16 to 32 only *Im3m* was found. It is worth to notice that no changes in the lattice parameter was found within each phase, meaning that added emulsifier do not swell the internal structure.

In the same study, addition of a lipophilic compound (R)-(+)-limonene to the ML/water system was proved to determine the transition to the hexagonal phase. Dispersion of bulk phase and stabilization of droplets at different emulsifier concentration resulted in hexosomes formation at all β values in the range of 2 to 32. Moreover, the lattice parameter was found to be constant at 5.82 nm; that means the polymer chains do not enter in the water channels of the structure and also that (R)-(+)-limonene molecules do not leave the liquid crystal phase to form a separate oil phase. As far as particle size is concerned, hexosomes radius was investigated for a system of (R)-(+)-limonene/ML/water with δ = 87, where $\delta = \frac{\text{mass of lipid}}{\text{mass of lipid+mass of oil}}$. The results showed that hexosomes radius R_H decreases as function of copolymer F127 content, from 152 nm at β=2 to 72 nm at β=36. This means that increasing quantity of emulsifier allows the stabilization of a larger surface, for a constant volume of lyotropic phase. The size decreasing behaviour is stronger at small F127 content and becomes less eminent for higher values of β, because of the difficulty to fragment smaller oil domains into particles. Furthermore, a trend in particles polydispersity could be observed: higher amounts of emulsifier do not only lead to smaller droplets but also decreases their polydispersity.

Finally, the effect of stabilizer on tetradecane-loaded monolinolein-based (δ = 66.7) micellar cubosomes was investigated. Clear micellar cubosomes were reported at β=4, while increasing Pluronic® F127 content to β=32 led to the progressive formation of EME. In accordance with the trend observed in hexosomes, the average particle size of the microemulsion resulted to be decreasing at high content of emulsifier, which allows to stabilize larger surfaces [31].

1.5.3 Sucrose stearate: a food-grade stabilizer

Even though copolymer F127 shows excellent stabilization performance, it cannot be used for direct application in food products as it is not food-grade. To overcome this drawback, Serieye et al. [30] explored the use of other a few emulsifiers allowed in foods. Sucrose stearate (S1670) and oleate (OWA-1570), sodium stearoyl lactylate (SSL), sodium caseinate (NaCas), whey protein isolate (WPI), lecithin and polysorbate 80 (Tween 80) have been chosen as candidates to replace Pluronic® F127 in order to formulate novel foods.

Table 1 reports the different values of particles size and stability time of the aforementioned emulsifiers. As expected, Pluronic® F127 offers very good colloidal stability over the whole experiment time (135 days), with an average particle size of 180 ± 4 nm. Sucrose stearate S1670 immediately appears to be best candidate to take over copolymer F127 in food products. In fact, its stability is equal to the one of F127 and the particle size is also comparable: 160 ± 3nm. Although NaCas and WPI also lead to droplets of similar size, they show very poor stabilizing effect over time with 40 and 7 days, respectively. As no antimicrobial agents were added to the formulation, NaCas may have been degraded upon bacterial growth, leading to particles destabilization. Lecithin was found to emulsify smaller droplets of 125 nm which were stable for a period of almost two months. Sodium stearoyl lactylate, Tween 80 and sucrose oleate are not suitable for novel food formulation due to their very short time stability.

In the same study, further investigation was conducted on the effect of stabilizers on particles' core structure after a poor-water soluble molecule was added. (R)-(+)-limonene/ML system stabilized by F127 was found to have coexisting presence of *Pn3m* and *Im3m* cubic phases, whereas S1670 did not affect the internal structure, leading to a single cubic phase, *Pn3m.* Sucrose stearate is a very small molecule compared with

triblock copolymer F127, thus has less effect on the internal nanostructure. Interactions of S1670 with the internal mesophase led to two remarkable facts: firstly, sucrose stearate do not change the nature of bicontinuous cubic phase. Only the *Pn3m* structure is present in S1670-stabilized cubosomes, whereas coexistence of *Pn3m* and *Im3m* was found when using Pluronic® F127. Secondly, at δ=60, the presence of two large polar sugar head groups results in a less negative mean curvature, giving raise to the formation of H_2 phase in place of L_2 phase [30].

Table 1. Particles stability (days) and average size (nm) for the different emulsifiers tested; δ=100, β=8% [30].

Emulsifier	**Average size [nm]**	**Stability [days]**
Pluronic® F127	180	> 135
Sucrose stearate (S1670)	160	> 135
NaCas	150	40
WPI	155	7
Lecithin	125	55
SSL	115	20
Tween 80	100	7
OWA-1570	100	1

Figure 1.8 shows the chemical structure of sucrose stearate (MW = 608.766 g/mol): an alkyl chain of 18 carbon atoms with no unsaturation (stearic acid) which is bounded to a sucrose molecule by an ester bond. This configuration leads to a very high hydrophilic-lipophilic balance of 15 and that means that sucrose stearate is better wetted in water and, thus, more suitable for stabilizing oil-in-water emulsion. As low molecular weight stabilizer, sucrose stearate shows a very good coverage of the particle surface: the hydrophobic heads form densely packed corona and ensure steric stabilization. This was also confirmed by Serieye et al. [30], they measured the zeta potential of limonene-loaded monoglycerides particles and found out that sucrose stearate-stabilized particles have a negative surface charge in the range of 10-15 mV, meaning that the type of stabilization can only be viewed as steric one, same as for Pluronic®. Moreover,

they concluded that the food-grade emulsifier has less impact on the internal structure of the particles than the largely used copolymer.

To my knowledge, due to such peculiar characteristics and its food-grade status (under "sucrose esters of fatty acids" (E473) in the CODEX Alimentarius), sucrose stearate appears to be the best candidate for the stabilization of mesosomes for novel food applications. In this work, its suitability for stabilising EPA-loaded monolinolein-based mesosomes is explored in terms of type of internal mesophase type, stability over time and particle size.

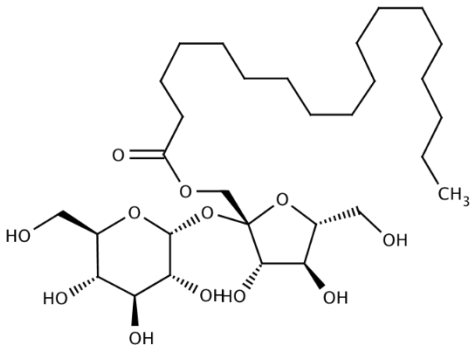

Figure 1.8. Schematic representation of the chemical structure of sucrose stearate.

1.6 Omega-3 fatty acids

1.6.1 Among n-3 polyunsaturated fatty acids: EPA and DHA

Long chain fatty acids normally have an even number of carbon atoms, in the range of 16-26. A further definition concerns the number of bonds between carbon atoms: if they only have single bonds along the hydrocarbon chain, they are called "saturated", whereas if they possess at least one double bond they are addressed as "unsaturated". In particular, monounsaturated refers to those fatty acids with only one double bond, while those with two or more are called polyunsaturated (PUFA). For example, eicosapentaenoic acid (EPA; 20:5) is an omega-3 (n-3) fatty acid with 20 carbon atoms and 5 *cis* double bonds (**Figure 1.10**). "n-3" refers to the position of the first double bond counting from the methyl (-CH_3) end of the molecule, in particular it is located between the third and fourth carbons. As the number of double bonds (degree of unsaturation) increases, the melting point decreases which confers the attribute of fluidity to PUFA.

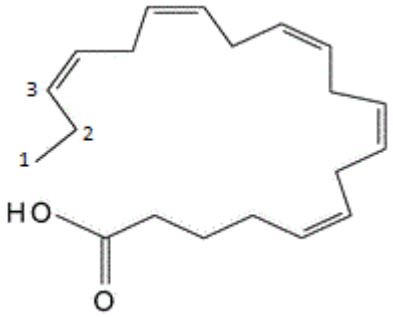

Figure 1.10. Representation of the structure of eicosapentaenoic acid (EPA; 20:5, n-3).

In the human body, eicosapentaenoic acid (EPA) and docosahexaenoic acid (DHA; 22:6) are synthesized from the n-3 precursor α-linolenic acid (ALA; 18:3) which is an *essential* fatty acid due to the fact that it cannot be synthesized endogenously. Theoretically, the ability to convert ALA to EPA and DHA means no need of ingestion of those compounds. However, there are at least two factors to be taken in consideration. Firstly, the enzyme δ-6-desaturase is involved in both pathways for omega-3 and omega-6 biosynthesis, which means possible competition for the conversion of different compounds. Secondly, many studies indicate that conversion of ALA (18:3n-3) to EPA (20:5n-3) and mostly DHA (22:6n-3) is quite inefficient. Researchers have shown that dietary supplementation of linseed oil (ALA) leads only to a moderate increase of only EPA plasma level, whereas the use fish oil (EPA + DHA) induces large presence of both compounds in plasma. Therefore, the total absence of omega-3 in the diet is likely to be a health disadvantage [32].

1.6.2 Sources of omega-3 fatty acids

Omega-3 FAs are primarily found in microorganisms that live in cold water. Microalgae (e.g. *Schizochytrium*) and Antarctic krill (*Euphausia superba*) represent the primary source of omega-3, which are then ingested by fish and consequently available for humans. Due to the high degree of unsaturation they have low melting point, thus they are fluid even at low temperature providing the necessary fluidity to biological membranes for life processes. Thus, the main source of n-3 fatty acids for humans is cold-water fish, such as salmon, mackerel, herring and tuna.

The main differences between marine sourced LC n-3 FAs are the different absolute amounts and the chemical bonds type. In unrefined raw fish oil, omega 3 FAs are largely present as triglycerides and in smaller amount as free fatty acids, whereas in krill oil, they are also bound in phospholipids in a considerable extent. Before being ready for consumption, raw fish oil has to undergo various purification processes which include degumming, deacidification, bleaching and deodorization. Such technological steps alter fatty acids composition and chemical bonds and, up to date, the exact distribution of omega-3 FAs among the different lipid types is not well known. Natural fish oil composition is around 18% EPA (20:5n-3) and 12% DHA (22:6n-3), which means that one omega-3 FA is present in each TG molecule, naturally bounded to the 2-position (*sn*-2) in TGs molecules. However, during re-esterification FAs are randomly redistributed, thus re-esterified triglycerides (rTG) contain equally distributed EPA and DHA molecules in *sn*-1/2 and -3 positions.

Esterification process is mainly used in order to increment n-3 FAs content. Firstly, TGs are chemically hydrolysed to free fatty acids and glycerol, subsequently FAs are transferred to ethylesters and enzymatically reconverted to triglycerides. Concentrate fish oil with EPA and DHA content up to 90% has been developed, and demonstrated to contain approximately 55-60% TG, 38-42% diglycerides and 1-3% monoglycerides [33].

1.6.3 Health benefits of omega-3

Dietary lipids are an essential macronutrient in all mammals as they are involved in several biological processes of homeostasis. Among lipids, fatty acids play a major role in cellular biological activities, in particular in n-3 and n-6 long chain PUFAs. These fatty acids are incorporated into the cell membrane and involved in several functions, such as providing fluidity and acting as precursors for eicosanoids synthesis. The latter group of molecules is known to play a central role in homeostasis, particularly in the inflammation regulatory system. In general, omega-3-derived eicosanoids have anti-inflammatory properties, whereas if they are synthetized from a different precursor, such as arachidonic acid (AA), they show pro-inflammatory nature. Moreover, EPA (20:5n-3) and DHA (22:6n-3) have been reported to be important precursors also for pro-resolving autacoids, resolvins, protectines and maresins, which are important compounds involved in the resolution of inflammation processes as they also possess

immune regulatory properties, such as shown in the decrease of leukocytes recruitment.

Anti-inflammatory properties are likely due to the fact that EPA and DHA consumption, in sufficient amount, has been proved to induce changes in the expression of 1040 genes, in particular decreasing the expression of 298 genes which regulate inflammatory- and atherogenic-related pathways [34]. As inflammation is known to be related to several chronic diseases, such as obesity, diabetes, rheumatoid arthritis, cancer, coronary heart disease and mental illness, it is of major interest to know how dietary compounds can modulate immune system response. Nowadays, Western diet is characterized by high n-6/n-3 PUFAs ratio (15:1 to 16.7:1) and that is reported to promote the aforementioned diseases. Lowering n-6/n-3 PUFAs ratio to 4:1 has been associate with 70% reduced mortality, in secondary prevention of cardiovascular diseases. Furthermore, a ratio of 5:1 resulted in positive effects in asthmatic patients and a ratio of 2-3:1 blocked inflammation in patients suffering rheumatoid arthritis [35]. Even though this data encourages a progressive decrease in the n-6/n-3 ratio of PUFAs consumption, it is important to know that the circulating ratio of omega-6 and -3 in human blood is 7:1. This result has been found by analysing phospholipids composition of white blood cells' membranes of 40'000 individuals. Therefore, it is logical to think that a correlation between the normal n-6/n-3 ratio of PUFAs and the desirable intake from food exists (James Smith, University of Leeds. Personal communication on the overview of fatty acids profile, with courtesy of EPIC consortium).

Inflammatory process has been also associated to the development of obesity-related metabolic disorders, such as hypertension, dyslipidemia and insulin resistance [35]. As far as insulin is concerned, however, positive results for insulin sensitivity were only measured in obese women with high inflammatory status at baseline, whereas other studies, for example the KANWU, showed no insulin sensitivity improvement in patients [36]. Despite the controversial results on insulin resistance, body weight control in general was found to be affected by n-3 PUFAs supplementation. Overweight patients who consumed a daily amount of 6g of tuna oil (rich in omega-3 FAs, approximately 1.9 g) for 12 weeks showed reduced body fat mass compared to a second group of patients who were given 6 g of sunflower oil [37].

Omega-3 fatty acids are also known to be essential for fetal development and healthy ageing, as they are important components of cell membranes and are particularly found in the brain and retina [38]. A study compared two groups of children whose mothers had DHA supplementation in one case (n = 29) and did not in the other (n = 15). Problem-solving skills of 9 months old children were better in the first group, with higher DHA intake [39]. A different study evaluated cognitive performance on 2.5 years old children after one group of mothers (n = 33) was given EPA + DHA supplementation during pregnancy and the second group (n = 39) was on placebo treatment. Children whose mother had omega-3 supplementation showed significantly higher scores for hand and eye coordination (114, SD 10.2) than those in the placebo group (108, SD 11.3) [40]. Furthermore, lower incidence of allergies has been reported in children whose mothers had adequate EPA and DHA intake during pregnancy and breastfeeding, probably associate with the anti-inflammatory properties of those compounds. As during pregnancy the fetus rely on nutrients which are transferred from the mother, also EPA and DHA intake depends on the mother having an adequate nutrition. Since 2010, dietary guidelines from the US Department of Health and Human Services suggest to pregnant women to eat 225-340 g of fish per week, which is equivalent to 300-900mg EPA+DHA/day, depending on the type of fish [38]. Differently, the European Food Safety Authority (EFSA) set a daily Adequate Intake[2] of 100-200 mg DHA for pregnant women in addition to the 250 mg EPA+DHA recommended for the adult population [36]. Most of mothers from US and Canada do not reach that amount of fish intake, neither do lots of European pregnant women, thus dietary supplementation may be an adequate solution [38, 41].

Even though scientific evidence shows that consumption of oily fish or dietary supplementation of EPA and DHA is correlated with lowered risk of mortality from coronary heart disease, there is not sufficient available data to derive an Estimated

[2] **Adequate Intake (AI)** is based on experimentally derived intake levels or approximations of observed mean nutrient intakes by a group (or groups) of healthy people. The AI for children and adults is expected to meet or exceed the amount needed to maintain a defined nutritional state or criterion of adequacy in essentially all members of a specific healthy population. When there is no sufficient scientific evidence to calculate an Estimated Average Requirement, Adequate Intake is used instead of a Recommended Dietary Allowance.

Average Requirement[3]. Therefore, EFSA experts' panel set an Adequate Intake for adults of 250 mg of EPA+DHA, which is considered a sufficient amount for secondary prevention for cardiovascular diseases. Moreover, an additional amount of 100-200 mg EPA+DHA has been advised to pregnant and breastfeeding women, and 100 mg of DHA supplementation has been recommended for infants from 6 to 24 months old. No specific directives have been given for the age period 2 to 18 years, thus children's omega-3 intake should be consistent with adults' advised intake [36].

In order to reach adequate amount of EPA and DHA ingestion, one of the possible solutions is omega-3 enrichment of food, and particular attention must be given to the bioavailability of the bioactive compound. In this perspective, the investigation of new delivery vehicles may have positive impact on the food business, leading to new sources with high content of n-3 polyunsaturated fatty acids. When marketing omega-3-enriched products is also important to remember that from a legislative point of view "*A claim that a food is a* ***source of omega-3 fatty acids****, and any claim likely to have the same meaning for the consumer, may only be made where the product contains at least 0,3 g alpha-linolenic acid per 100 g and per 100 kcal, or at least 40 mg of the sum of eicosapentaenoic acid and docosahexaenoic acid per 100 g and per 100 kcal.*", whereas to claim that is **high in omega-3** "*…the product contains at least 0,6 g alpha-linolenic acid per 100 g and per 100 kcal, or at least 80 mg of the sum of eicosapentaenoic acid and docosahexaenoic acid per 100 g and per 100 kcal*." (Reg. (EC) N° 1924/2006 of the European Parliament and of the Council on nutrition and health claims made on foods. Amended by: Commission Regulation (EU) No 116/2010 of 9 February 2010).

1.7 Lipid digestion and mesophases implications

1.7.1 Long-chain fatty acids (omega-3) digestion and uptake

On average, a Western adult has a daily intake of lipids of about 100 g, of which 92-96% are long-chain triglycerides. In order to be absorbed, TGs need to be hydrolysed to two free fatty acids and one monoglycerides. Once ingested, fats enter the stomach and are

[3] **Estimated Average Requirement (EAR)** is the average daily nutrient intake level estimated to meet the requirements of half of the healthy individuals in a group.

roughly dispersed, mainly thanks to stomach peristalsis and partially due to gastric lipases. Subsequently, droplets reach the upper small intestine, where they are finely emulsified by biliary salts, cholesterol and phospholipids secreted by the gall bladder, also with the help intestinal peristalsis. The formation of an emulsion is an important prerequisite for pancreatic lipases to cleave ester bonds between FAs and the glycerol backbone. In fact, the presence of bile salts is recognized to be very important for the solubilization and the transport of digested products to the absorption sites, thus bringing them away from the oil droplet surface, making the latter more accessible to lipases. In particular, pancreatic lipases together with cofactor co-lipase anchor the oil droplets and hydrolyse *sn*-1 and *sn*-3 ester bonds and produces *sn*-2 monoglycerides. Lipolysis is a very fast process which is usually completed when lipids move from the duodenum to the jejunum, where lipids uptake occurs [22, 33, 42, 43].

Compounds absorption is known to take place in the enterocytes. Particularly, the cell membrane of the apical moiety of enterocytes is folded into villi which are further characterized by the presence of microvilli. This structure greatly enhances the absorptive surface of the small intestine and it is named Brushed Border Membrane (BBM). Together with mucus and glycocalyx, microvilli constitute a unique microclimate: the unstirred water layer (UWL). As this is a polar environment, lipophilic compounds are poorly soluble, thus they are prevented from reaching the enterocytes' cell membrane. However, products of lipid digestion, biliary phospholipids and cholesterol self-assemble in a variety of different microenvironments, such as liquid crystalline phases, mixed micelles and micelles. These species highly increase intestinal solubility of lipophilic molecules, prevent their precipitation and facilitate their transfer through the UWL. The UWL has low pH due to an efficient antiport exchange of H+/Na+ which leads to micellar dissociation and long-chain fatty acids protonation when pH becomes lower than fatty acids pKa. Protonation facilitates LCFAs uptake, which mainly occurs by passive diffusion, a high-capacity low-affinity mechanism. Passive diffusion efficiency strongly depends on the cell ability to maintain a favourable long-chain FAs concentration gradient between the intestinal lumen and the intracellular compartment. Lipopolysaccharide Binding Proteins (LBP) have also been considered to be involved in active lipid absorption, however their contribution is still debated. Within

the enterocytes, LCFAs are then reconverted to triglycerides and assemble into chylomicrons, ready to continue the metabolic route [33, 44, 45].

1.7.2 Lipid mesophases formation during digestion

The fact that digestion products, such as monoglycerides and fatty acids, together with biliary phospholipids and cholesterol self-assemble into structured mesophases might be a key point for the formulation of novel foods. Using lyotropic liquid crystalline phases as delivery vehicle is thought to increase bioavailability of poorly water-soluble molecules because those particular structures conformation resembles steps of fat digestion. In fact, whilst pancreatic lipases act on oil droplets, different lipid mesophases have been reported to appear. Thus, it is the colloidal species that form after lipid digestion the actual "carrier" of poorly water-soluble compounds that people normally ingest. Given that, mesosomes convey guest molecules to a digestive stage which closer to lipid uptake that conventional emulsions do, providing great advantage in terms of availability. Moreover, they have great solubilization capacity, which is essential in the food industry as (i) the amount of bioactive compound to be delivered is usually larger than that of drugs, and (ii) due to regulatory issues, the quantity of emulsifier in food products must be kept as low as possible. It has been proved that the encapsulation efficiency of the anti-cancer agent 20(S)-protopanaxadiol in monoolein cubosomes stabilized by poloxamer 407 is 90%, which means that most of the drug was encapsulated in the nanoparticles [46].

The presence of liquid crystalline phases in the GI tract is well known, even though most of the work has focused on the molecule composition during digestion instead of on colloidal structure. In this perspective, *in vitro* digestion of triolein emulsions has been reported to give rise to particles with self-assemble internal structure. With time of lipase action many different liquid crystal species appear, transforming the oil-in-water emulsion to a microemulsion (EME) and further to an inverse micellar cubic (*Fd3m*), hexagonal (H_2) and bicontinuous cubic (*Pn3m* or *Im3m*) phases, as shown in **Figure 1.11**. At the end of the digestive process, vesicles are the most present species under the condition of the study [47].

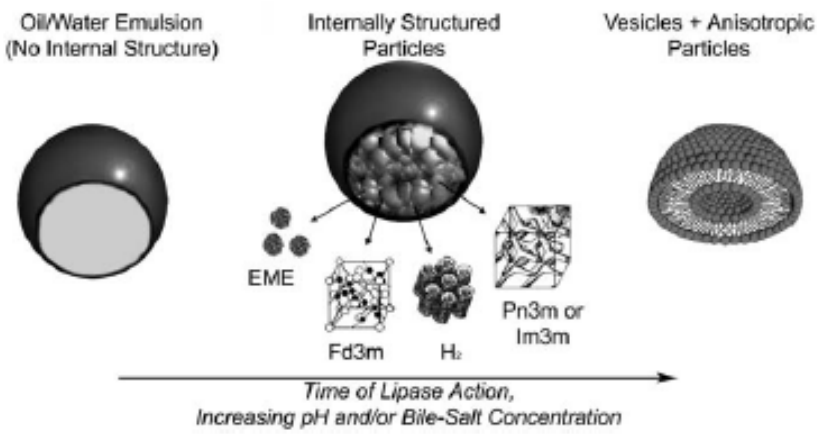

Figure 1.11. Schematic figure of phase transitions during lipid digestion. From the oil-in-water emulsion depicted on the left-hand side, microemulsion (EME), inverse micellar cubic phase (Fd3m), inverse hexagonal phase (H_2), inverse bicontinuous cubic phase (Pn3m or Im3m) and finally vesicles are reported to appear with time of lipases action under the condition of this study. Figure reproduced from [46].

A study on lyotropic liquid crystal nanoparticles formation during milk digestion also support the formation of those structure in the just mentioned order. This *in vitro* experiment in presence of pancreatin at low bile salt concentration (triglycerides/bile salt = 33.6, triglyceride/pancreatin = 0.175) demonstrated that after 1 minute of milk digestion the transition from emulsion to emulsified microemulsion occurs. Further digestion showed the appearance of the inverse hexagonal phase with a lattice parameter of 6.4 nm, after 6 minutes. After 9 minutes, hexagonal structure diminishes a bit and partially remains until the end of digestion. When lipases act for more than 11 minutes cubosomes are also present and formation of vesicular structure on their surface begins, whereas after 30 minutes (completed digestion) vesicles dominate. At higher concentration of bile salts, the structure is led towards more hydrophilic phases, due to increased swelling of the internal aqueous region, this means that milk digestion is faster at higher concentration of bile salts [43].

Very promising results during milk digestion investigation were also found when in vitro digestion was conducted in absence of bile salts. 1 minute of lipase action already showed the appearance of an emulsified microemulsion (EME), which undergo transition to *Fd3m* inverse micellar cubic phase after 2 minutes (60% digested

triglycerides). At 2.5 minutes, a hexagonal structure with lattice parameter of 5.6 nm appears and vanishes later, at 15 minutes. From 10 minutes onwards, the inverse cubic phase *Pn3m* also coexists with H_2 and lasts until complete digestion. Its lattice parameter varies from 21.7 nm at the beginning to 20.0 nm after 20 minutes. The formation of such structures during fatty meal digestion (milk) in absence of bile salts is of extremely importance because it is likely to facilitate lipid digestion in bile-compromised individuals. In fact, the formation of the highly porous cubic structure allows to keep apolar compounds in solution and the high surface area of the bicontinuous phase greatly improve accessibility of lipases. Therefore, quantitative important digestion may still occur in bile-compromised individuals [43].

Furthermore, not only the novel nanocarriers resemble natural lipid digestion structure, they also show bioadhesive characteristics and enhanced permeability in intestinal cells. Due to their size in the nanoscale, cubosomes can be absorbed by pinocytosis which ends in the invagination of the cell membrane and vesicle formation. The process is energy depended and saturable, in addition absorption rate is affected by carriers' size and surface properties. Increased bioavailability of 20(S)-protopanaxadiol-cubosomes compared with the raw drug was attributed to the fact that the self-assemble bilayer of cubosomes is very similar to the cell membrane structure, thus, it is reasonable to think that the nanocarriers can be transported intact through the cell membrane. Even though this mechanism has not been proven, it is sure that mesosomes possess great solubilisation capacity which allow to cross the UWL and bring the bioactive compounds close to the enterocytes membrane [46].

2 Objective

Lipid liquid crystalline mesophases are largely found in nature: they exist in organelles such as the Golgi network and mitochondria, during exocytosis, endocytosis, viral fusion, cell division and many others [28]. Above all, they have been observed to occur during lipid digestion, in the gut lumen [42, 43, 47, 48]. The efforts towards the formulation of lipid nanoparticles for nutraceuticals delivery is therefore built on the idea of mimicking the structures that naturally form upon digestion in the human body so that bioavailability in greatly enhanced. This is expected to be particularly true in case of poorly-water soluble compounds which are not well retained in the intestine and cannot easily cross the unstirred water layer to reach the enterocytes, due to their hydrophobic nature.

In the pharmaceutical industry, some products are already delivered by means of lipid nanoparticles (e.g. Amphotericin B-Albelcet, AmBisome and benzoporphyrin-Visudyne) [49]. Besides encapsulation and sustained release of drugs, these particles have attracted interest for nutraceuticals solubilization, chemical degradation protection and delivery. Their importance is not only limited to healthy issues, they are indeed promising for aromas and flavors solubilization and controlled release, bio-sensor and (enzymatic) bio-reactors carriage and control of membrane protein crystallization. Although these are just few examples of the copious number of use, these nanoparticles are suitable for various fields of application. Last but not least, such lipid nano-devices are non-toxic and biodegradable, which makes them perfectly suitable for any environmentally-friendly application [15, 26, 49, 50].

As far as the food industry is concerned, research is also conducted aiming to create or improve innovative and more efficient ways to deliver nutrients and bioactive compounds with positive health effects, focusing on targeted release and increased bioavailability. Nanotechnology is a key element to pursue these goals as it has already given significant improvement for drugs and therapeutic components delivery. Although very promising for food applications, pharmaceutical nanotechnologies need to be re-designed in terms of food regulations. With these premises, this work aims to explore the use of food-grade liquid crystalline nanoparticles for the delivery of eicosapentaenoic acid (EPA), as representative compound of a very important class of

molecules: omega-3 fatty acids. Their role in cellular functions is widely recognized among scientists and public opinion as omega-3 fatty acids provide fluidity to cell membranes, are involved in the inflammation regulatory system, are acknowledged to lower blood pressure and protect against cardiovascular diseases. Furthermore, they have been recognized to influence gene expression with possible direct impact on the development of inflammatory-related chronic diseases such as obesity, diabetes and mental illness. Moreover, they are known to be crucial for fetal growth and healty ageing [34, 38].

Even though lots of research has focused on the improvement of nanoparticle structuring for pharmaceuticals delivery, only little effort has been made as far as the food sector is concerned. In fact, to create a stable aqueous dispersion of lipid nanoparticles, the triblock co-polymer Pluronic® F127 is mostly used among studies. Although it is FDA approved, it cannot be used in food products. In January 2017, Serieye et al. [30] published a paper about the stability throughout time of limonene-loaded monoglycerides nanoparticles with many different food-grade stabilizers. Sucrose stearate appeared to be the best candidate to substitute Pluronic® F127, due to their comparable stabilization properties [30], therefore it has been chosen to investigate the formulation of eicosapentaenoic acid (EPA)-loaded nanoparticles.

In order to move a step forward in the design and use of smart food-grade delivery vehicles, this work focused on understanding the impact of EPA on the well-known monoglycerides/water system by creating a phase diagram of the bulk oil phase EPA/monoglycerides in excess of water. Based on this knowledge, specific nanoparticle dispersions were designed and studied in detail. I note, that modification of the internal crystalline arrangement may happen when bulk phases are dispersed. Here, particle-surfactant interactions are likely to induce phase changes. For example, the stabilizer Pluronic® F127 induces swelling of the inner nanostructure and under some conditions induces a phase change. In order to better understand the effect of different stabilizers on the internal structure of the nanoparticle, three different dispersions have been prepared at different concentrations, based on which seemed to be the most representative ones. Samples have been made in duplicates, using both the new-entry sucrose stearate and the well-known Pluronic® F127 stabilizer, so that a better

comparison could to be guaranteed. The nanoparticles were analyzed in terms of their internal structure by using Small Angle X-ray Scattering (SAXS) technique and concerning their stability by means of Dynamic Light Scattering (DLS).

3 Investigation techniques and materials

3.1 Small angle X-ray scattering (SAXS)

3.1.1 SAXS principle

X-ray scattering is a structural characterization tool that has affected many different research fields. It makes use of the variety in electron density of a sample to generate contrast and detect the internal structure of materials on a nanoscopic/atomic scale. **Figure 3.1** illustrates the basic components of an X-ray scattering instrument. The source irradiates the sample which is positioned on a sample holder, the collimation system defines the zero-angle position and assures a narrow beam, the beam-stop avoids that the incident and very intense X-ray beam hits the detector and the detector measures the intensity as well as the position of the incoming scattered X-rays. X-ray scattering techniques provide reciprocal space data. Thus, a variation of electron density at a nanometre length scale scatters X-ray beams to low angles, while at an atomic length scale the beams are scattered to wide angles. Therefore, SAXS techniques are used to study material structures in a range of 1 to 100 nm size, while Wide Angle X-ray Scattering (WAXS) is used to investigate molecular/atomic structures.

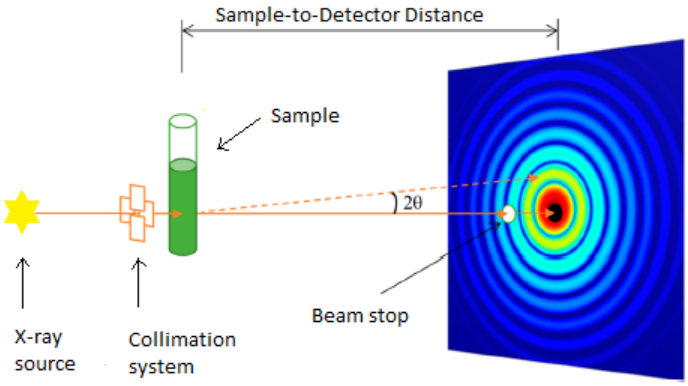

Figure 3.1. Schematic figure of the components of an X-ray Scattering instrument. Figure adapted from [47].

When X-rays hit atoms, they are scattered and they finally reach the detector. The interference pattern at the detector can be constructive (in phase), destructive (out of phase) or at an intermediate interference phase, depending on the observation angle

2θ between the incident direction and the scattered X-rays direction. On the detector in **Figure 3.1**, constructive interactions are shown as a bright circle, whereas destructive waves cancel each other, shown as dark blue areas. A 2D-pattern forms on the detection plane as result of the interference and the intensity of the waves is measured as function of the scattering angle 2θ. The interference pattern is specific for the internal structure of the sample. The position of every pixel is measured as function of the X-rays wavelength λ and the scattering angle 2θ:

$$q = \frac{4\pi}{\lambda} \cdot \sin\theta \qquad (2).$$

where q is the scattering vector and expressed as [1/nm]. When particles align into highly ordered and periodic (crystalline) structures, specific scattering pattern with pronounced peaks are recorded. These diffraction peaks are called “Bragg peaks” and the position of maximum intensity is defined by their scattering vector q_{peak}. Each reflection peak is characterized by the Miller indices, which describe directional and planar orientation of the crystalline structure that give rise the corresponding peak. They are integer digits identified by the letters *h*, *k*, and *l* and indicated within round brackets: (*hkl*). Each triplet of digits refers to a particular set of crystal planes with a given orientation within the unit cell [50]. The repeated distance of a stack of diffracting planes can be derived from Bragg’s law

$$d_{hkl} = \frac{2\pi}{q_{hkl}} \qquad (3).$$

The so-called d-spacing (d_{hkl}) is geometrically related to the Miller indices as function of *a*, the lattice parameter of the crystalline structure, that is the dimension of the *unit cell* of the crystal. The relevant crystalline arrangements for this work regard the hexagonal and cubic Bravais lattices, which relationships with d_{hkl} and *a* are

hexagonal[4]

$$\frac{1}{d_{hkl}^2} = \frac{4}{3}\frac{h^2 + k^2 + hk}{a^2} \quad (4),$$

and cubic[5]

$$\frac{1}{d_{hkl}^2} = \frac{h^2 + k^2 + l^2}{a^2} \quad (5).$$

Due to constructive/destructive interactions between scattered X-rays, only some of the repeating structures of crystals are detected in SAXS analysis, as reflection peaks, and they appear at specific proportional distances based on the crystals' space group. The ratios between the reflection peaks of the most relevant biological lipid mesophases are well known and reported in **Table 2**.

Table 2. Reflection laws of the most relevant biological liquid crystals. The integer numbers represent the permitted *hkl*-reflections for each specific space group. They are calculated as $h^2 + k^2 + l^2$ for the cubic structures and as $h^2 + k^2 + hk$ for the hexagonal structure.

	Reflection laws	
L_α	$\left(\frac{d}{d(h)}\right) = 1,2,3,4, \ldots$	***d*** is the repeat distance of the layers
Cubic (*Im3m*)	$\left(\frac{a}{d(hkl)}\right) = 2,4,6,8,10,12,14 \ldots$	***a*** is the lattice parameter of the crystals
Cubic (*Pn3m*)	$\left(\frac{a}{d(hkl)}\right) = 2,3,4,6,8,9,10 \ldots$	
Cubic (*Iad3*)	$\left(\frac{a}{d(hkl)}\right) = 6,8,14,16,20,22, \ldots$	
H_2	$\left(\frac{\sqrt{3}a}{2d(hk)}\right) = 1,3,4,7,9, \ldots$	
Cubic (*Fd3m*)	$\left(\frac{a}{d(hkl)}\right) = 3,8,11,12,16,19,24, \ldots$	

[4] Only the lattice parameter of the hexagonal section is considered in the H_2 structure, thus the relationship is reported in terms of the lattice parameter α, independently from rods length.

[5] Valid for all the cubic phases of interest for this work: bicontinuous (*Im3m, Pn3m, Ia3d*) and micellar cubic.

In order to calculate the lattice parameter of the structure from the scattering pattern, the relations

$$q = \frac{4\pi}{a \cdot \sqrt{3}} \cdot \sqrt{h^2 + k^2 + hk} \tag{6}$$

and

$$q = \frac{2\pi}{a} \cdot \sqrt{h^2 + k^2 + l^2} \tag{7}$$

are derived from equations (3) - (4) and (3) - (5), for the hexagonal and cubic phases, respectively. Finally, by plotting the scattering vector *q* of the various peaks against the corresponding values from the reflective laws in **Table 2**, a linear regression is obtained which slope is used to calculate the lattice parameter *a* of the hexagonal

$$a = \frac{4\pi}{\sqrt{3} \cdot slope} \tag{8}$$

and cubic

$$a = \frac{2\pi}{slope} \tag{9}$$

mesophases.

In case of the lamellar phase, q_h is proportional to 1,2,3… . Differently, due to the disordered state of particles which do not give rise to a single repeat distance, the inverse micellar L_2 phase is identified by the characteristic distance only, $d = 2\pi/q_{max}$, where q_{max} is the position at maximum intensity of the nearest neighbour correlation peak [50, 51, 52, 53].

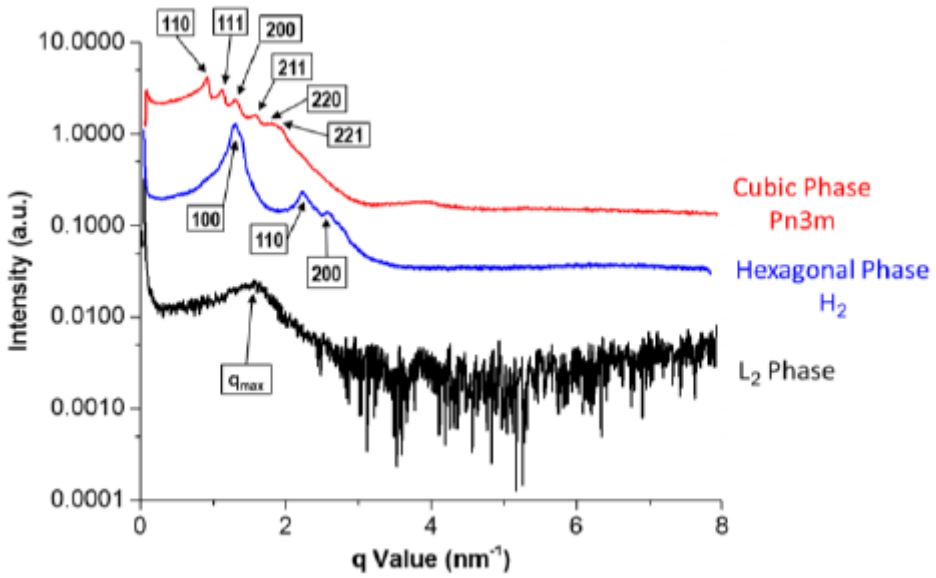

Figure 3.2. Example of scattering patterns for the cubic (Pn3m), the hexagonal and the micellar phases. The Miller indices of the reflection peaks are reported, as well as the value q_{max} in case of the micellar phase. Figure reproduced from [14].

3.1.2 SAXS instrument, set-up and data treatment

The experiments have been partially conducted with the Anton-Paar (Austria) SAXSpace instrument at the School of Food Science and Nutrition (FS&N at the University of Leeds, UK). The equipment consists of a SEIFERT (The Netherlands) X-ray generator, which is operated at 40kV and 50 mA with a sealed-tube Cu anode. The source provides X-ray radiations with wavelength λ = 0.154 nm. The collimation system ensures that the beam is narrow and focused on the sample. The scattered X-rays are recorded 1D-Mythen detector form DECTRIS (Switzerland), where the energy input is translated in functional data.

Some of the samples have been run at "Diamond Light Source" synchrotron (Didcot, UK). Small and Wide Angle X-ray Scattering equipment is located at the beamline I22 where experiments were carried out using X-ray wavelength of 0.69 Å and energy of 18 keV; Sensor-to-Detector Distance was 3.74 m. Bulk phase samples are gel-like, thus they were spread on a spacer whereas dispersions were put in capillaries and placed in a capillary holders. Both apparatus have a jacket where water flows from a thermostat, as temperature control system. Exposure time was incredibly shorter than for the

Anton-Paar instrument: bulk phase samples were exposed for 0.1s whereas concentrated dispersions for 5s because they diffracted poorly compared to the others. Data reduction was carried out by DLS specialists, afterwards peak analysis was completed the same way as for data from the other machine.

During the first part of the work, the phase diagram of the bulk system Dimodan®/EPA/water was completed, starting from previous work of two students of the School of FS&N. As the sample consisted of a gel-like material a *paste cell* was used as holder and it was placed at a sample-to-detector distance (SDD) of 317 mm, height 0 mm and rotation angle 0°. δ = 98, δ = 90 and δ =73 samples were measured at different temperatures, from 15 to 65° C with 10° C interval. Using the Anton-Paar instrument, 30 minutes holding-time was set for the sample to reach the desired temperature and 3 frames of 20 minutes each were taken for the measurements; no beam absorber was used. δ = 70, 68, 65 were measured in a second moment at the synchrotron and δ = 98 and 73 were repeated to have better diffraction. Exposure time was 0.1s.

In the second part of this study, the bulk phase was dispersed using two different stabilizers. Investigation on the internal structure of the nanoparticles was conducted to understand how the stabilization agent influenced the system. As the dispersion was made at 1% solids concentration, the sample was firstly concentrated with centrifuge filters and later pipetted into a *capillary* holder. Only three specific concentration were chosen to be investigated, those samples were position at SDD of 317 mm, height 0 mm and rotation angle 0°, as previously. Experimental temperatures were chosen based on the expected purposes of the nanoparticles: chilled or room temperature storage and human consumption. Each sample was measured at 5° C (as representative of a chilled environment), 25° C (room temperature) and 37° C (during consumption/digestion). δ = 98 dispersions were analysed with the equipment at the University of Leeds: holding-time of 30 minutes was set for the temperature to stabilize and 3 frames were measured for 60 minutes each. δ = 85 and δ = 73 samples measurement was carried out at the synchrotron, with exposure time of 5s.

After the scattering pattern was recorded, the raw data was treated with *SAXS Treat* firstly and *SAXS Quant*, in case of data from the Anton-Paar instrument. The first software was used to calibrate the primary peak's position, the latter to complete data

reduction, including normalization and background subtraction. Data analysis was then concluded by identifying the q values of the reflection peaks and plotting them against the reflection peaks ratio showed in **Table 2** in order to assure the correct identification of the mesophase and the calculation of the lattice parameter. Water channels size can also be evaluated to better understand interactions of guest molecules and stabilizers with monoglycerides. Using equations

$$r_w^{Pn3m} = 0.391a - l_c \quad (10)$$

$$r_w^{Im3m} = 0.305a - l_c \quad (11),$$

the water channel radius can be easily calculated if the lattice parameter α and the alkyl chain length (l_c) of the most representative amphiphile are known [5, 28].

Data treatment procedure was identical for both the bulk and the dispersed phases.

3.2 Dynamic light scattering (DLS)

3.2.1 DLS principles

Dynamic light scattering is one of the most used techniques for particles size measurement. It is based on the principle that small particles diffuse more rapidly than large ones. Correlation between particles diameter and their diffusion rate is described by the Stokes-Einstein equation

$$D_H = \frac{k_B T}{3\pi\eta D} \quad (12),$$

where D_H is called hydrodynamic diameter[6], k_B is the Boltzmann constant, T the absolute temperature, η the viscosity of the solvent and finally D is the diffusion coefficient which describe how fast the particles diffuse.

When a monochromatic light beam (laser) shines onto a solution, particles in Brownian motion scatter the radiations which intensity is then measured at the detector.

[6] **Hydrodynamic diameter** is defined as the diameter of a hard sphere that has the same diffusion coefficient D as the particle being measured.

Scattered light can be *in phase* or *out of phase*, causing either bright or dark areas with different intensities. As particles are in Brownian motion, the interference pattern changes constantly and the rate of movement is correlated to the particle size distribution by equation (11). The analysis of the intensity fluctuation throughout time allows to calculate the correlation function which contain the information about the diffusion coefficient to be used in the Stokes-Einstein equation. That information is extrapolated by using the cumulants analysis and allow to determine mean size, z-Average[7] and the polydispersity index[8] (PdI) of the particles) [54, 55].

3.2.2 DLS instrument, set-up and data treatment

Particles size was measured by using a Zetasizer Nano (Malvern Instruments Ltd., UK). Basic components of DLS instrument are a laser (He-Ne, wavelength λ = 633 nm), a photon counting device and a digital signal processor. Measurements were carried out at 25 °C, at fixed scattering angle of 173° and each measurement cycle included 11 runs of 10s. As refractive index of the material, 1.488 was used, as representative of monolinolein [56].

Several measurements were taken within the 42 days of time stability investigation. Each one of the six samples was diluted to 10^{-3} % solids and the measurement was repeated 3 times. z-Average and PdI were calculated as the average of the 3 measures and plotted against the number of days elapsed since sample preparation. Waterfall plots were also made in order to highlight how particles size distribution varies throughout time, in terms of volume (%).

3.3 Materials and samples preparation

3.3.1 Chemicals

During this research food-grade Dimodan®® U/J (DU) was used as monoglycerides (98%) mixture, which hydrophobic tails composition is 91% C18 chains. In particular, C18:2 chains are the major component (62%), followed by C18:1 (24.9%) and C18:0 (4.2%). The other 2 % is represented by di-glycerides, free fatty acids and antioxidants. It is

[7] **z-Average** is the intensity-weighted mean diameter obtain from the cumulants analysis.
[8] The **Polydispersity Index (PdI)** is a dimensionless value of the broadness of the size distribution and it is derived from the cumulants analysis.

manufactured by Danisco Co Ltd. (Denmark) and was stored at a temperature of 4 °C. Ethanol absolute of 99.98% v/v was used to solubilize the monoglycerides (purchased from VWR international S.A.S (France).

20% w/v solution of eicosapentaenoic acid (EPA) in ethanol, produced by Cayman Chemical Company (USA), was used as representative of fish oil. EPA content of this product has a purity of 98% or greater and it is only suitable for research purpose. It needs to be stored at -20 °C and away from light as the polyunsaturated alkyl chain is very much prone to oxidation.

Pluronic® F127 was purchased from Sigma-Aldrich (USA). It consists of a tri-block copolymer with two hydrophilic moieties bounded to a hydrophobic one. It has a molar weight of about 12600 gr/mol and the HLB is in the range of 18-23. Pluronic ® F127 is stored at room temperature, in a cool and dry place.

Sucrose stearate was chosen as alternative stabilizer with food-grade status. The one used during this research was manufactured by Glentham Life Sciences Ldt (UK), with only research purposes. Its molecular weight is 608.75 gr/mol and HLB = 15. It comes as white to off-white powder with 75% purity in monoesters and, particularly, a purity in monostearate greater than 70%. Sucrose stearate is also stored in cool and dry place, at room temperature.

Throughout the whole research, deionised water prepared with Milli-Q purification system (Millipore UK Ltd, UK) was used.

3.3.2 Preparation

In order to complete the phase diagram of the DU/EPA system, different samples were prepared at three specific concentrations of the two components: δ65, 68, 70, 73, 90 and 98; where δ is defined as

$$\delta = \frac{DU}{DU + EPA} \qquad (13).$$

δ65, 68, 70 were 73 were chosen to try to find a clear inverse micellar cubic phase (*Fd3m*), δ90 concentration needed to be repeated because inaccurate in previous works

and at δ98 the inverse bicontinuous cubic phase (*Pn3m*) was sought, otherwise it was only present in absence of EPA, at δ100.

After the necessary calculation were made, DU monoglycerides were weighed on an electronic scale and then dispersed in ethanol to obtain a 2% w/v DU stock solution. The mixtures of DU and EPA at different concentrations were then prepared in 6 ml glass vials and the ethanol evaporated in a vacuum oven, at room temperature. Afterwards, deionised water was added to reach a dilution of 10% w/w solids in case of δ98 concentration, 30% w/w solids at the other concentrations. The samples were agitated on a Heidolph reax control mixer at 2500 rpm for 30 seconds and then heated up to 50 °C and cooled down in an ice-cold water bath: 4 cycles of temperature variation were conducted in order to assure complete mesophases structuring. A soft gel formed and it was spread on a paste cell for SAXS analysis, which was conducted at six different temperatures from 15 to 65 °C with 10 °C intervals. δ65, 68, 70, 73 and 98 were ran at the synchrotron, whereas the other two at the University of Leeds.

The second part of the research focused on the dispersed mesophases. Three different δ concentrations were chosen, one for each type of structured liquid crystalline phases that was found during the previous experiments: δ98 as representative of the bicontinuous cubic phase, δ85 of the hexagonal one and δ73 of the micellar cubic phase. SAXS analysis was carried out to investigate the internal structure of the nanoparticles, in order to evaluate if they undergo any changes upon dispersion, with different stabilizers. Instead, DLS measurements were conducted to assess particles size and their stability throughout time. These two experiments were performed on the same samples, which were made as following: duplicates of δ98, δ85 and δ73 samples were obtained by co-dissolving monoglycerides from a stock solution of 20% w/v DU solubilized in ethanol and EPA from the solution manufactured by Cayman Chemical Company (USA). The solvent was then evaporated at room temperature, using a vacuum oven. In the meantime, two solutions were prepared: one of 8 % w/w Pluronic® F127 and the other of 8 % w/w sucrose stearate (mass of stabilizer/mass of oil phase %). In order to facilitate the stabilizer to reach the oil water interface, the samples were heated up at 50 °C to make sure the lipid phase was completely melted and each stabilizer solution was pipetted into three samples while they were agitated with a

magnetic stirrer. Deionised water was added in order to reach a final concentration of ϕ = 1% w/w solids (0.1 g of lipids in 9.9 g aqueous solution at δ98 and δ85, 0.08 g of lipids in 7.92 g aqueous solution at δ73). Finally, the samples were realized by fragmentation using ultrasonic waves without external cooling. Sonication was applied for 13 minutes (3' at 60 % amplitude + 10' at 80%) with pulse mode 2s on/1s off.

In order to obtain a clear scattering pattern from the SAXS analysis the samples were concentrated by evaporating the water at room temperature, with the help of the vacuum oven. SAXS analysis was then carried out partially at the University of Leeds and at Diamond Light Source synchrotron. Instead, for particles size measurements in DLS, the samples were diluted 10 times in order to reach a final concentration of 10^{-3} % solids.

A more complete description of the analysis settings can be found in sections 3.1.2 and 3.2.2.

4 Results and discussion

4.1 Phase diagram of the monoglycerides/EPA/water system

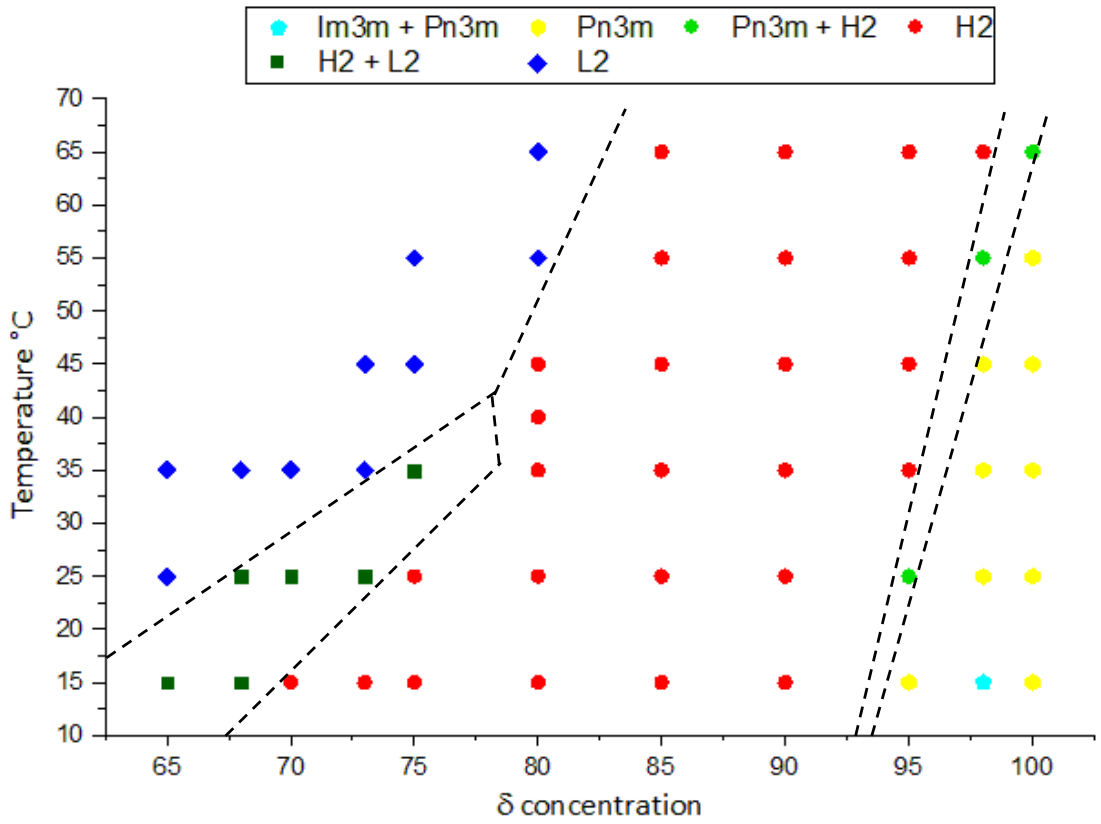

Figure 4.1. δ-T phase diagram of a Dimodan® U/ EPA mixture in excess of water. Phase transition boundaries are identified by the dashed line.

In order to fully comprehend the effect of eicosapentaenoic acid content on the self-assembly properties of a monoglycerides mixture, the phase diagram for the Dimodan® U/EPA/water system was completed. This research has taken over two previous studies that investigated the same system. Raw data from [13] and [57] were personally elaborated and new datasets at different concentrations were collected for a better understanding of phase transition boundaries.

Monoglycerides/EPA ratio is expressed in terms of δ (equation (10)), as this is largely comparable with other works. Raw data of δ 80 was taken from [13] and δ 100, 95, 85, 75 from [57]. In addition, δ90 and δ 70 were remade due to the lack of accurate results

and δ 98, 73, 68, 65 were added to better understand the phase transitions from the bicontinuous cubic phase *Pn3m* to the hexagonal phase at higher δ values and from H_2 to the micellar cubic *Fd3m* at lower δ values.

As represented in **Figure 4.1** pure monoglycerides (δ = 100) of the mixture Dimodan® U self-assembly into a reverse bicontinuous cubic structure with space group *Pn3m,* when they are fully hydrated (excess of water). Such arrangement is found from a temperature of 15 °C to 55 °C, whereas at 65 °C also the reverse hexagonal phase weakly appears and the two phases coexist. This is due to the fact, that raising temperature progressively enhances the mobility of the alkyl chains, which leads to an increased chain volume thus leading to an increase of the chain splay (higher value of the CPP). Interesting to note that this leads also to an effective dehydration of the head groups at polar/apolar interface, however it is not the driving force for the increasing CPP. This temperature driven trend is also confirmed by the analysis of the lattice parameter: its value continuously decreases from 10.05 nm at 15 °C to 7.50 nm at 65 °C. No further investigations at higher temperatures have been conducted in this work but, considering the findings of others [26, 58], it is legitimate to assume that the presence of the hexagonal phase becomes progressively stronger, until it is replaced by the inverse micellar phase at even higher CPP.

In presence of 2% of the guest compound EPA (δ = 98), the transition from the inverse cubic (*Pn3m*) phase to the inverse hexagonal phase is seen at 55 °C, 10 °C lower than at δ = 100, as deducible from the superimposed appearance of both scattering patterns. At 65 °C phase transition is completed and only the H_2 phase is present. EPA is highly unsaturated and its melting point is -54 °C; these factors contribute to increase the negative curvature of the lipid layers, promoting the formation of a highly curved bilayer surface. The result at 15 °C is in discordance with the correspondent at δ = 100 because the two inverse bicontinuous cubic phases *Im3m* and *Pn3m* appear to coexist in case of δ = 98. The space group *Im3m* exists at less negative curvature and it is more likely to appear, when the monoglycerides have a smaller chain splay, i.e. in the presence of other molecules (guests or stabilizers) that promote smaller curvatures (molecules with lower CPPs). As stated before, EPA drives the system towards the formation of hexagonal phase replacing the bicontinuous cubic ones, thus it is very surprising to find

the *primitive* space group *Im3m* in that context. δ = 98 sample was made during this project, whereas data for δ = 100 is taken from a previous work, therefore this disagreement is most probably due to preparation inaccuracies. The trend of the lattice parameter meets the expectations; it is 9.69 nm in the *Pn3m* structure at 15 °C and decreases progressively to 7.83 nm at 55 °C. Moreover, it is slightly smaller than the one found at δ = 100 which is between 10.05 and 7.86 nm at the same temperatures. This trend can be attributed to the increase of the chain splay and to the expulsion of water from the water channels, which lead the structure to shrink and the lattice parameter to become smaller. H_2 phase coexists with the *Pn3m* phase at 55 °C and has a lattice parameter of 5.79 nm which reaches 5.65 nm at 65 °C

At δ = 95, the inverse *diamond* cubic phase is only present at 15 °C, whereas at 25 °C it coexists with the H_2 phase during phase transition. At 35 °C, only the hexagonal structure is found and it persists up to the maximum investigated temperature of 65 °C. The lattice parameter *a* of the cubic structure has a value of 8.54 and 8.39 nm respectively, whereas the hexagonal one shrinks from 5.99 to 5.32 nm at 25 and 65 °C, respectively. Once again, the values are in accordance with the foreseen behavior at higher EPA content and increasing temperature. At δ = 90 and δ = 85, the phase diagram is dominated by the presence of the hexagonal phase throughout the whole temperature range. As aforementioned, the lattice parameter *a* changes depending on EPA content and temperature. At δ = 90, *a* = 5.97 nm at the lowest temperature and decreases to 4.92 nm at 65 °C, while at EPA concentration of δ = 85 *a* decreases from 5.34 down to 4.77 nm.

The hexagonal phase is still predominant at δ = 80, up to 45 °C. However, the scattering pattern at 45 °C shows three more poorly-defined and small peaks that may be due to a weak coexists with the inverse micellar cubic phase *Fd3m*. Although the latter is not perfectly clear, it has been found in previous works in a similar range of temperature and guest molecule content. For example, soy phosphatidylcholine (SPC)/glycerol dioleate (GDO) mixture shows transition from H_2 to Fd3m when they are mixed in ratio 50:50 to 45:55 at 25 °C, before it undergoes transition to the L_2 phase[9] [26] and

[9] Transition temperature and δ value are dependent on the lipid and guest molecule nature.

limonene content of 40% in the monolinolein/water system induces the formation of the inverse micellar cubic phase as well [58]. For this reason, the *Fd3m* phase has been searched in the hexagonal to inverse micellar L_2 phase boundary regime; further, the sample was analysed also at 40 °C. However, no strong evidence of the cubic micellar structure was detected, even though some very weak peaks are present together with the H_2 diffraction pattern.

At δ = 75, the hexagonal arrangement is found at 15 and 25 °C. Again, the *Fd3m* phase is not present during the transition from H_2 to L_2 phase. The latter coexists with the hexagonal phase at 35 °C and it is present as pure L_2 phase at 45 and 55 °C. The very fast transition from one phase to the other may be due to the strong effect of temperature on the omega-3 fatty acids: as stated before, the melting point of EPA is -54 °C. Therefore, at room temperature its fluidity is greatly enhanced and so is the chain splay. The inverse cubic micellar phase may be present in a very limited temperature and δ value range within the phase diagram area. Although the diffraction pattern for T = 65 °C was not present in the dataset of the previous work, it has not been repeated during this work due to the fact the no further changes in the structure are expected once the L_2 phase is formed.

Samples δ = 73, 70, 68 and 65 have been analyzed at "Diamond Light Source" synchrotron (Didcot, UK) at the SAXS beamline I22. The intermediate δ value 73 and 68 samples were studied, because at that δ range monoglycerides self-assembly structures were expected to show greater polymorphism. In particular, the inverse cubic micellar phase was expected to appear at some δ-T combinations. Therefore, due to the unstable nature of the *Fd3m* phase, the investigated δ intervals were narrowed down to try to isolate the cubic micellar structure. At δ = 73, the monoglycerides mixture self-assemblies into the hexagonal phase at 15 °C. It undergoes phase transition at 25 °C, at which temperature the H_2 phase co-occurs with the inverse micellar L_2. The latter is then observed alone at 35 °C and 45 °C and no traces of *Fd3m* phase are visible in the scattering patterns of this mixture at these conditions. No further investigations were conducted at even higher temperatures, as there is no more possible phase change once the L_2 phase is formed.

The last three EPA/monoglycerides/water samples show the same behaviour: the transition occurs from hexagonal to inverse micellar phase with no formation of the cubic micellar one. At δ = 70, the pure H_2 phase is present at the first temperature measurement and transforms to L_2 phase, when increasing the temperature. At 35 °C the phase transition is completed, after phase coexistence at 25 °C. Increasing the EPA content to δ = 68 leads to a more negative surface curvature that determines the coexistence of hexagonal and inverse micellar phases at already 15 °C. At 35 °C the lipid structure completely assemblies into the L_2 phase. The last concentration that has been investigated was at δ = 65. At this condition, only traces of the H_2 structure are present at 15 °C, while the characteristic first form-factor maximum of the inverse micellar structure appears already to be predominant in the scattering pattern. At higher temperatures only the L_2 phase is present. The blank area on the top-left corner of the phase diagram in **Figure 4.1** is not explored experimentally, but can be entirely assigned to the L_2 phase, since there is no stronger curved mesophase existing. Note, as matter of fact, the highest mean curvature possible is given for a sphere.

As far as the lattice parameter is concerned, the decreasing trend at increasing EPA content and raising temperature is confirmed. At δ = 80 it goes from 5.13 to 4.83 nm at 45 °C, while moving to lower δ (higher EPA content) the lattice parameter decreases to a minimum of 4.66 nm at δ = 65 (T =15°C). It is important to note that the inverse micellar phase does not display crystalline order, but rather a characteristic distance *d* can be identified in the first form-factor maximum of the SAXS pattern. Its position represents an estimate for the average next-nearest neighbor distance of the disordered micelles. In this work, its value results to be between a maximum of 4.09 nm at δ = 73 (T = 35 °C) and a minimum of 2.99 nm at δ = 80 (T = 65 °C). From the results, the characteristic distance of the inverse micellar phase appears to be affected more by the increasing temperature than by the increasing EPA content. In fact, the minimum value is seen at 65 °C even when δ is as high as 80. Deceasing δ to 65 only determines a characteristic distance of 4.06 nm, at 15 °C. This means that the dehydration effect of the polar heads caused by high temperatures is stronger than the chain splay increase effect provoked by the amount of EPA. It is reasonable to assume that the characteristic distance of the micelles at δ = 65 and T = 65 °C is smaller than 2.99 nm.

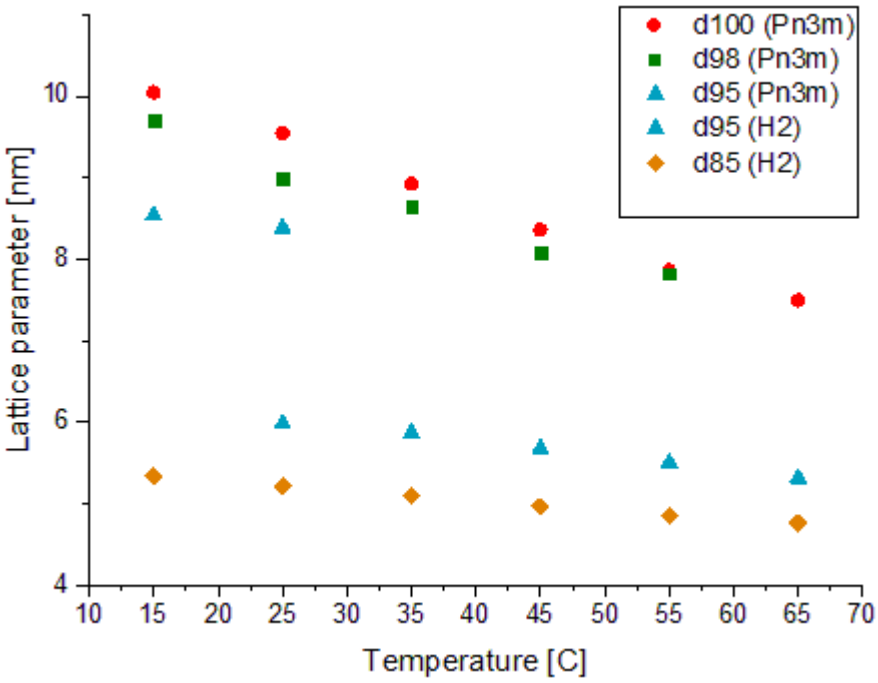

Figure 4.2. Variation of the lattice parameter as function of temperature of four representative δ values.

Figure 4.2 shows how the lattice parameter changes for the most significant phases and concentrations. Taking a closer look at the bicontinuous cubic lattice trend, it appears to decrease faster than in the case of the hexagonal one. In fact, at δ = 100 it goes from 10.05 to 7.50 nm with an average decrease rate of 0.051 nm/°C and with a rate of 0.0374 nm/°C, at δ = 98. Instead, in case of the hexagonal structure, the lattice parameter decreases almost four time slower, with an average rate of 0.013 nm/°C at δ = 95 and of 0.011 nm/°C at δ = 85. This behavior may be due to the packing of monoglycerides in the two different structures: in the H_2 phase the amphiphiles are closely packed to form a smaller structure compared to the bicontinuous phases. Molecular packing constraints in the discontinuous H_2 phase are likely to limit bigger changes in the water radius (less significant swelling variations), and hence hamper steeper decreases in lattice parameter.

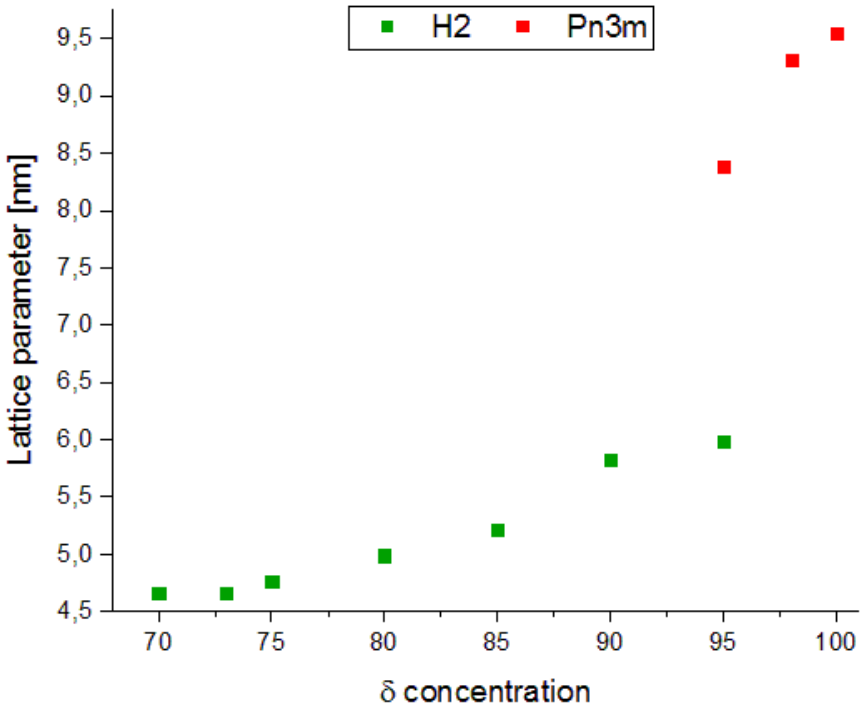

Figure 4.3. Lattice parameter variation at different lipid composition, depending on the type of mesophase. Temperature = 25 °C.

Similar conclusions can be drawn for the relation between EPA content and lattice parameter. **Figure 4.3** shows how the lattice parameter changes in function of δ depending on the type of mesophase, at 25 °C. In case of inverse bicontinuous cubic structure, the lattice parameter *a* varies from 9.54 nm at δ = 100 to 8.39 nm at δ = 95, that corresponds to a rate of 0.23 nm/δ decrease. In contrast, *a* of the hexagonal phase shrinks from 5.99 nm at δ = 95 to 4.66 nm at δ = 70 indicating a variation of 0.05 nm/δ. Again, such behavior can be explained in terms of different molecular packing conditions given in continuous and discontinuous phases, respectively.

4.2 Dispersed nanoparticles characterization

Three samples with each stabilizer were prepared at different concentrations in order to be compared. Pluronic® F127 and sucrose stearate were the two candidates chosen based on the results of Serieye et al. [30]. Samples were sonicated as described in section 3.3.2: fine and homogeneous dispersion were obtained, as shown in **Figure 4.4**. X-ray experiments were carried out both, with the SAXS equipment at the University of Leeds (Leeds, UK) and at "Diamond Light Source" synchrotron (Didcot, UK).

Measurements were taken at three different temperature, representative of refrigeration temperature (5 °C), room temperature (25 °C) and body temperature (37 °C).

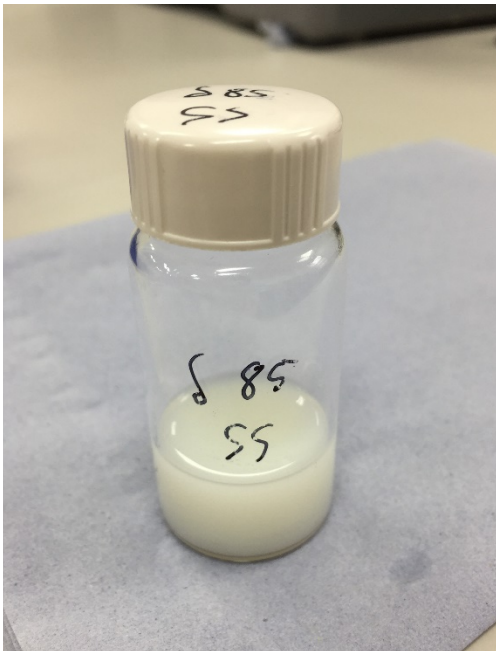

Figure 4.4. Example of a nanoparticle dispersion with δ = 85 and stabilized with sucrose stearate.

Data of δ = 98 concentration was collected at the SAXS laboratory at the University of Leeds. From the SAXS analysis, both Pluronic® F127 and sucrose stearate stabilized particles resulting to have an inverse bicontinuous cubic internal structure with the space group *Im3m*. This mesophase appears at higher hydration level compared to *Pn3m* and it is characterized by a less negative surface curvature; in this case it is due to the interactions with the stabilizing molecules. As far as the triblock co-polymer is concerned, the hydrophobic moiety of PPO acts as an "anchor" in the lipid domain, while the hydrophilic chains extend in the water aqueous region, covering the surface and providing steric stabilization of the colloidal particles. Differently, sucrose stearate is formed by an alkyl chain which extend into the lipid layer of the structure and by a large polar head group that forms a dense corona around the particles, ensuring steric stabilization.

Pluronic® F127 was already known to affect the internal structure of particles. Guillot et al. [31] found out that increasing stabilizer content leads space group change from *Pn3m* to *Im3m*. In particular, this transition is almost completed at 8% stabilizer content, which is the quantity used in this work. Moreover, Chong et al. [4] describe how the internal structure is particularly influenced by the co-polymer, when the lipid core is given by glycerol monooleate. In contrast, the *Pn3m* symmetry is maintained in the case of using monolinolein. In the context of this work, a monoglycerides mixture is used, thus the effect of the stabilizer is different. Serieye et al. [30] compared Pluronic® F127 and sucrose stearate, and based on their finding, the latter does not affect particles internal structure, at least not in presence of pure monolinolein.

On the contrary, the results of this work show that sucrose stearate greatly influences the assembly properties. Same as the triblock co-polymer, sucrose stearate modifies the space group from *Pn3m* to *Im3m* and, in addition, it significantly affects the lattice parameter. **Table 3** reports the values of the lattice parameter a, the type of phase and the water channel diameter, $D_w = 2\ r_W$, calculated with equations (10) for *Pn3m* and (11) for *Im3m* phases, respectively (using $l_c = 15.7\ \mathrm{nm}$ [28]). Even if Pluronic® F127 modifies the internal structure, the lattice parameter values are in line with the Bonnet transformation relationship, which predicts $a_{Im3m}/a_{Pn3m} = 1.279$ [10], in binary bulk systems [31]. In fact, the ratio between *a* values of the *Pn3m* and the *Im3m* phases (δ = 98, T = 25 °C) is 1.403, which is in reasonable agreement with the theoretical value considering that the conditions are quite different. Much different is the ratio in case of sucrose stearate stabilized particles: $a_{Im3m}/a_{Pn3m} = 1.824$ [11], which indicates the structure of the *Im3m* phase greatly swollen with respect to the *Pn3m* phase. Omitting the difference from the theoretical value that is due to the system conditions, the great difference between the two particles is likely to be caused by sucrose stearate molecules being absorbed into the water channel. Sucrose stearate molecule is about 20 times smaller than the triblock co-polymer and can penetrate into the water channel

[10] δ = 98 and T = 25° C: a_{Im3m} = 12.62 nm for Pluronic® F127 stabilized nanoparticles, a_{Pn3m} = 8.99 nm in bulk phase

[11] δ = 98 and T = 25° C: a_{Im3m} = 16.40 nm for sucrose stearate stabilized nanoparticles, a_{Pn3m} = 8.99 nm in bulk phase

and acts as a chaotrope, which leads to less curved structures, as it is known to happen for co-surfactants (amphiphilic molecules) [7].

Table 3. Pluronic® F127 and sucrose stearate stabilized particles (δ = 98) are compared in terms of lattice parameter, type of mesophase and water channel diameter (D_w), at three different temperatures.

Sample	Temperature [°C]	Lattice parameter [nm]	Phase	D_w* [nm]
Sucrose stearate, δ=98	5	18.59	*Im3m*	8.2
	25	16.40	*Im3m*	6.9
	37	14.50	*Im3m*	5.7
Pluronic® F127, δ=98	5	13.61	*Im3m*	5.2
	25	12.62	*Im3m*	4.6
	37	11.91	*Im3m*	4.2

*$D_W = 2\ r_W$ (using Equation 11).

Water channel diameter is also an important factor, when as the objective of particle structuring is to incorporate functional guest compounds to be delivered. In case of Pluronic® F127 stabilized particles, the diameter of the water channels varies about 1 nm, i.e. from 5.2 nm at 5 °C to 4.2 nm at 37 °C. Much larger is the variation when sucrose stearate is used as stabilizing agent: from 8.2 to 5.7 nm, a variation of 2.5 nm. If room temperature is considered as storage condition, the lattice parameter differs of 2.3 nm between the two stabilizers: *a* is 4.6 nm in case Pluronic® F127 is used, which is in line with the typical water channel size of bicontinuous phases [28], and 6.9 nm using sucrose stearate.

The difficulty of tuning nanoparticles' properties and the inability to create highly swollen structures to load large compounds are two of the major bottlenecks for the exploitation of lyotropic liquid crystalline nanocarriers. For example, they could be used as transporter for enzymes. In that case, water channel diameter is fundamental as enzymatic protein size is in the range of few nanometers; note, even few decimals could make the difference between the possibility to load a molecule or not. Water channel shrinking phenomena at elevated temperatures may also be used as a trigger for guest compounds release. When temperature increases hydrophilic guest molecules are expelled, if they do not fit in the channels network anymore.

Table 4. Lattice parameter and type of mesophase are shown for each sample the was measures, at three different temperatures. "*" refers to coexisting phases.

Sample	Temperature [°C]	Lattice parameter [nm]	Phase
Sucrose stearate, δ=98	5	**18.59**	*Im3m*
	25	**16.40**	*Im3m*
	37	**14.50**	*Im3m*
Pluronic® F127, δ=98	5	**13.61**	*Im3m*
	25	**12.62**	*Im3m*
	37	**11.91**	*Im3m*
Sucrose stearate, δ=85	5	**17.89**	*Fd3m*
	25	**17.74**	*Fd3m*
	37	**17.65**	*Fd3m*
Sucrose stearate, δ=73	5	**18.10**	*Fd3m*
		5.96*	H_2*
		4.24*	L_2
	25	**18.01**	*Fd3m*
		5.88*	H_2*
		4.26*	L_2*
	37	**17.90**	*Fd3m*
		5.81*	H_2*
		4.24*	L_2*

Samples with δ = 85 and δ = 73 have been measured at "Diamond Light Source" synchrotron. Despite the high brilliance of the SAXS beamline I22, no good results have been collected for Pluronic® F127 stabilized particles at those concentrations, as attested by their absence in **Table 4**. One reason may be particle size. In fact, sucrose stearate stabilized particles were much bigger than Pluronic® F127 ones at the time of the measurements, while they are significant smaller directly after the particle formation (**Figure 4.5**). The low number of structural repetitions within each particle[12] might prevent to obtain a well ordered liquid crystal and hence no clear diffraction pattern is observed. Another factor to take into account is that none of the samples diffracted at ϕ = 1 % w/w concentration. The samples were concentrated by using a vacuum oven that might have compromised the samples. In fact, the samples had different evaporation times, probably due to water affinity of the surfactant and lipid

[12] As particles size at the time of the measurement was in the range of 150 – 170 nm and their lattice parameter might have been in the order of 10-20 nm, the number of repeated unit cells within the particles and the crystalline structural order might have not been sufficient to give a good diffraction pattern.

composition. In case of Pluronic® F127 stabilized particles, there was no standardized procedure to apply to this preparation step and no similar practice in literature, thus samples might have been dehydrated too much and the structure collapsed.

As shown in **Table 4**, nanoparticles which are stabilized with sucrose stearate and have EPA content of δ = 85 are found to have inverse cubic micellar internal phase with a lattice parameter that varies from 17.89 nm at 5 °C to 17.65 nm at 37 °C. Even though the reflection law for the *Fd3m* space group is fulfilled by the peak positions, the result is unexpected. The most predictable structures would have been the hexagonal and the bicontinuous cubic phase with *Pn3m* space group. In fact, the H_2 phase is found in the in the bulk samples at the same conditions (**Figure 4.1**), whereas the *Pn3m* phase can be expected, when taking into consideration also the presence of the surfactant sucrose stearate, which tends to decrease interfacial curvature. The formation of the *Fd3m* phase could have been caused by the treatment in the vacuum oven that promotes the dehydration of the structure, thus more negative surface curvatures, driving the self-assembly process towards the formation of micellar phases.

At δ = 73, three different mesophases can be distinguished within the investigated temperature range: hexagonal, inverse cubic micellar and inverse micellar structures are present. Although the H_2 phase diffracts only weakly, two peaks are clearly visible and their positions are in accordance with the reflection laws. The lattice parameter at 5 °C is 5.96 nm, and it decreases as expected, when temperature raises, reaching a value of 5.81 nm at 37 °C. Regarding the *Fd3m* phase, two to three peaks that fulfill the reflection law can be identified in different frames. The lattice parameter varies from 18.10 to 17.90 nm at 5 and 37° C, respectively. A pronounced lobe is also present in each scattering pattern of the δ = 73 samples indicating the coexistence of L_2 phase. I note that a three-phase coexistence is against the classic Gibbs phase rule and can only be explained by non-homogenously dispersed particles, i.e., coexisting particle populations with slightly differing compositions. In contrast, the bulk phase diagram (**Figure 4.1**) displays at δ = 73 a phase transition from H_2 to L_2 within the temperature range 15 to 45 °C. Although the *Fd3m* was expected to form under bulk phase conditions due to findings of other authors [26, 58], it was somewhat surprising to be observed in the dispersion instead, because the applied surfactant/stabilizer actually decreases

interfacial curvature. I note that the presence of the *Fd3m* phase is of particular interest because it mimics the initial steps of lipid digestion [43].

4.3 Time stability of dispersed nanoparticles

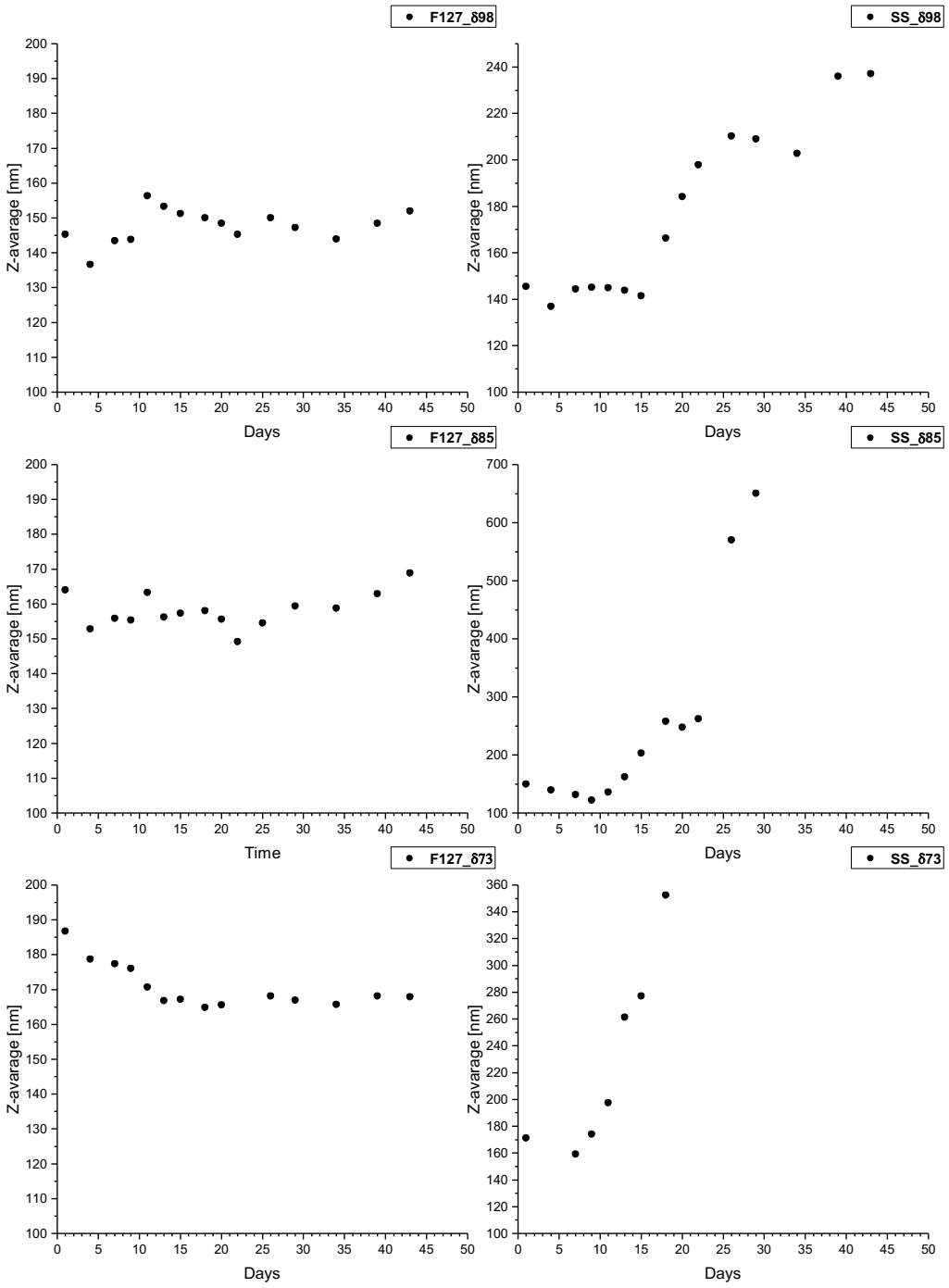

Figure 4.5. Time stability comparison of Pluronic® F127 and sucrose stearate stabilized dispersions (left to right) at δ = 98, δ = 85 and δ = 73 concentrations (top to bottom).

In **Figure 4.5**, the Z-average (nm) is plotted against time (days) to show the particles' stability and thus the potential shelf life of a nanoparticles-containing product. Samples δ = 98, δ = 85 and δ = 73 of Pluronic® F127 stabilized nanoparticles are shown on the left-hand side indicating that the dispersions are stable up to 42 days. The triblock co-polymer is largely used in pharmaceutical applications and it has been attributed great stabilizing effect. Serieye et al. [30] reported a stability of over 135 days of a sample with δ = 100 concentration and of at least 15 days in case of limonene-containing particles. They also obtained the same results, when the dispersions were stabilized with sucrose stearate, which was accredited to be the best candidate to replace Pluronic® F127 for food-related purposes.

In this work, stability was measured throughout 42 days and showed important differences between the two surfactants. Pluronic® F127 stabilizes all three dispersions (δ = 98, δ = 85 and δ = 73) throughout the entire period of time, with an average diameter of 147.7 nm, 158.1 nm and 170.8 nm, respectively. Sucrose stearate gives the best results with the δ = 98 sample, which is stable for 14 days with an average diameter of 143.1 nm, followed by the δ = 85 dispersion being stable for 10 days (138.9 nm particle size), and last, the δ = 73 sample is only stable for 8 days (average particle diameter of 168.1 nm). A reason for the very short stabilizing properties of sucrose stearate on the EPA/monoglyceride mixture is that eicosapentaenoic acid is liquid already at -54 °C, thus there is a high probability for the formation "point defects" in the liquid crystalline matrix, which may act as contact spots between particles to undergo coalescence [6].

Although the particle size is only stable for a limited number of days, the δ = 98 and δ = 85 samples show a peculiar behaviour: the particle size increases until it reaches a new stable size, which is maintained for few days before undergoing complete destabilization. The δ = 98 sample stabilizes a second time with sizes of about 200-210 nm for 12 days (from day 21 to 33), whereas δ = 85 stabilizes with sizes around 250-260 nm from day 17 to 21 before particle sizes rapidly increase up to 650 nm on day 28. The δ = 73 sample destabilization is much faster than for the other two. Also, no similar trend can be seen: Z-average diameter reaches 352 nm after 17 days, and after that, the dispersion undergoes phase separation and oil droplets become visible in the vial.

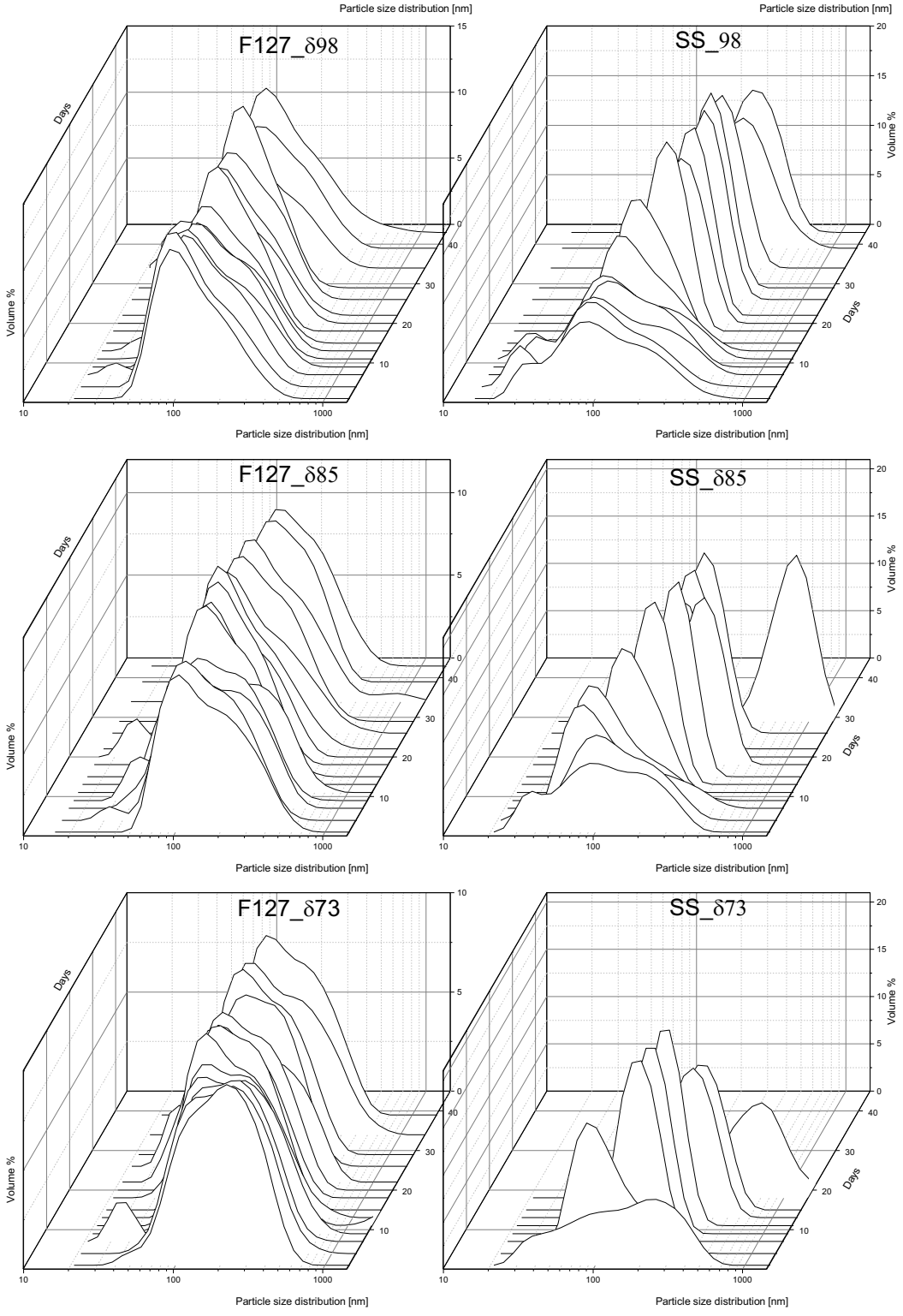

Figure 4.6. Waterfall plots of Pluronic® F127 and sucrose stearate stabilized dispersions (left to right) at δ = 98, δ = 85 and δ = 73 EPA load (top to bottom). Particle size [nm] is on the x-axis, % volume distribution of particles is on the y-axis and time [days] in on the z-axis.

Figure 4.6 shows how volume distribution of particles changes during the 42 days of analysis. The ones on the left (smaller particles sizes), describe time stability of the Pluronic® F127 stabilized samples. Here, no visible shift to greater particles sizes is present, meaning that the average particle size does not change as it was already found from the Z-average analysis. However, looking at the curves of the latest days of measurements, it is possible to see a widening trend of the curves, due to the increase of the polydispersity. The plots on the right-hand side refer to sucrose stearate stabilized nanoparticles: a maximum-shift to greater particles sizes is visible when the dispersions destabilize. Remarkably, an unexpected trend is seen with regards to the curves width: at the three concentrations, the size distributions become narrower displaying also greater amplitudes, which indicates the emulsion becomes more monodispersed with time.

5 Conclusions

In order to reproducibly engineer food-grade delivery vehicles with defined liquid-crystalline internal structure, it is necessary to understand how guest molecules affect the self-assembly properties and how the surfactant further modifies the structure. The objectives of this work were the study of phase behavior of eicosapentaenoic acid/ monoglycerides mixture in excess of water and the investigation of a food-grade stabilizer to create edible nanoparticles for nutraceutical delivery.

Main reasons for the utilization of lipid nanoparticles with ordered internal structure were given by (i) the great similarity of the engineered particles with the self-assembled colloids which naturally form in the intestine during lipid digestion, that is expected to improve nutraceutical bioavailability, (ii) the high loading capacity that is provided by the water channel network (in case of inverse cubic and hexagonal phase), (iii) the possibility to solubilize both lipophilic and hydrophilic guest compounds and by (iv) the opportunity to tune internal structure, giving different characteristics in terms of controlled release and stability [3, 6, 43].

The first part of the study provides insight into phase behavior of swollen eicosapentaenoic acid/monoglycerides mixtures in water. As expected, the phase diagram in **Figure 4.1** shows that EPA molecules induce high curvature structures from bicontinuous cubic towards inverse micellar, following the order $V_2 \rightarrow H_2 \rightarrow Fd3m \rightarrow L_2$. This is mainly due to the high unsaturation degree of the EPA molecule and their relatively small head group, both leading to a higher CPP value.

Further, temperature effects on the phase behavior of the lyotropic liquid crystals were studied. Strong effects on the lattice parameter have especially been observed for the bicontinuous phases. The *Pn3m* phase displays lattice parameter decrease of 0.05 nm/°C and 0.037 nm/°C at δ = 100 and δ = 98, respectively. At higher EPA concentrations temperature has also significant influence. At δ = 75 the L_2 phase forms between 35 and 45° C, whereas, at smaller δ values, it appears at room temperature already.

Having a phase diagram of the EPA/monoglycerides system at hand, allowed to choose what seemed to be the most interesting loading concentrations for the design of dispersed particles. δ = 98 was chosen in order to investigate the formulation of a

cubosome-based dispersion, δ = 85 was related to the hexagonal phase, thus the formation of hexosomes were expected, and δ = 73 was studied with the intent of producing micellar cubosomes. The latter dispersion has found great attention [30, 31, 59] and it is particularly interesting because it is the first colloidal form present during lipid digestion. The possibility to tune particle's internal structure allows to create particles with different properties and function. For example, hexosomes show a slower hydrophobic compound release compared to cubosomes and a three-times better bioavailability of the drug cinnarizine [60]. Differently, water channel size of cubosomes can be swollen up to 21.8 nm (lattice parameter of 47.0 nm) by the incorporation of charged lipids [28] which allows loading and delivery of much larger compounds compared to hexosomes or micellar cubosomes.

With regards to this work, both Pluronic® F127 and sucrose stearate stabilized particles show *Im3m* internal structure at δ = 98. However, the lattice parameter was quite different in the two cases: the triblock co-polymer forms a thick corona all around the particles but do not penetrate the water channels because of its large size (MW 12600 gr/mol). In fact, the lattice parameter value is in accordance with the Bonnet transformation relation which is $a_{Im3m}/a_{Pn3m} = 1.279$ and it is found to be 1.403[13]. When particles are stabilized by sucrose stearate, the pore size is approximately 37% larger than in the case of Pluronic® F127. The increase in water channel diameter is caused by sucrose stearate molecules penetrating inside the aqueous network and acting as chaotrope, thus inducing the structure to swell. Equivalent results are reported by Sun W. et al. [27] that engineered a liquid crystalline structure with space group *Pn3m* that can absorb up to 52% of water, by using a mixture of monoglycerides and sucrose stearate. In this case, the sucrose ester was only used for the purpose to swell the nanostructures and gave excellent results.

Remarkably, nanoparticles with a composition of δ = 73 have shown a rich polymorphism: H_2, *Fd3m* and L_2 phases are all present at all the investigated temperatures. It is interesting to note that these structures have also been found during milk fat digestion.

[13] This value indicates a slight swelling of the *Im3m* phase.

Despite interesting results in terms of particles internal structure, sucrose stearate did not meet the expectations in terms of stabilization capacity. Findings of the present work are far from those obtained by Serieye et al. [30]: they stabilized a dispersion of self-assembled monoglycerides (δ = 100) for over 135 days and limonene-loaded particles for 15 days. EPA loaded particles appear to have similar time stability, if the omega-3 fatty acid is present in small amounts. Only δ = 98 sample is stable for 15 days from preparation, while δ = 85 for 11 days and δ = 73 for 9 days. EPA content clearly affects time stability in a negative way; it would be very interesting to investigate the behaviour using different guest compounds, in order to understand how the nature of the molecule influences stability of dispersions.

Even though stabilization of EPA-loaded nanoparticles using sucrose stearate leads to a limited hypothetical shelf-life, application for this product can still be interesting to fortify food products with very short shelf-life such as fresh milk and fresh fruit juice. Further work in this direction can lead to application in a much broader variety of fresh products such as soups and beverages in general. Study on bioavailability of delivered nutraceuticals is also to be conducted but the premises are very good as nanoparticles internal assembly mimics the structures that normally form during fat digestion and simplify their absorption.

6 Appendix

Table 5. Values of the slope (reflection law – peaks position) and lattice parameter of the investigated EPA/monoglycerides mixtures.

	Temperature [°C]	Slope	Lattice parameter [nm]	Phase type
δ = 100	15	0.63	10.05	*Pn3m*
	25	0.66	9.54	*Pn3m*
	35	0.70	8.93	*Pn3m*
	45	0.75	8.36	*Pn3m*
	55	0.80	7.86	*Pn3m*
	65	0.84	7.50	*Pn3m*
δ = 98	15	0.50	12.48	*Im3m*
		0.65	9.70	*Pn3m*
	25	0.70	8.99	*Pn3m*
	35	0.73	8.66	*Pn3m*
	45	0.78	8.09	*Pn3m*
	55	0.80	7.83	*Pn3m*
		1.25	5.80	H_2
	65	1.28	5.65	H_2
δ = 95	15	0.74	8.54	*Pn3m*
	25	0.75	8.39	*Pn3m*
		1.21	5.99	H_2
	35	1.24	5.87	H_2
	45	1.28	5.68	H_2
	55	1.32	5.51	H_2
	65	1.36	5.32	H_2
δ = 90	15	1.21	5.97	H_2
	25	1.25	5.82	H_2
	35	1.29	5.62	H_2
	45	1.33	5.44	H_2
	55	1.37	5.29	H_2
	65	1.48	4.92	H_2
δ = 85	15	1.36	5.34	H_2
	25	1.39	5.22	H_2
	35	1.42	5.10	H_2
	45	1.46	4.97	H_2
	55	1.49	4.86	H_2
	65	1.52	4.77	H_2
δ = 80	15	1.41	5.13	H_2
	25	1.45	4.99	H_2
	35	1.49	4.87	H_2
	45	1.50	4.83	H_2
	55	1.50	4.83	H_2
		1.83	3.43	L_2
	65	2.10	2.99	L_2
δ = 75	15	1.50	4.83	H_2
	25	1.52	4.76	H_2

	35	1.53	4.73	H_2
		-	-	L_2
	45	1.49	4.23	L_2
	55	1.53	4.12	L_2
				H_2
δ = 73	15	1.54	4.70	H_2
	25	1.56	4.66	H_2
			trace	L_2
	35	1.53	4.09	L_2
	45	1.58	3.98	L_2
δ = 70	15	1.55	4.68	H_2
	25	1.56	4.66	H_2
			trace	L_2
	35	1.56	4.03	L_2
δ = 68	15	1.55	4.68	H_2
			trace	L_2
	25	1.55	4.67	H_2
		1.53	4.10	L_2
	35	1.55	4.06	L_2
δ = 65	15	1.56	4.66	H_2
		1.53	4.11	L_2
	25	1.55	4.06	L_2
	35	1.57	4.00	L_2

Table 6. Z-Average mean (three measurements) and standard deviation (SD) of Pluronic® F127 stabilized dispersion during time stability investigation.

	Pluronic® δ = 98		**Pluronic® δ = 85**		**Pluronic® δ = 73**	
Days	Mean	SD	Mean	SD	Mean	SD
1	145.3	4.744	164	3.092	186.7	5.311
4	136.6	2.715	152.8	5.534	178.7	2.307
7	143.4	0.9074	155.9	1.058	177.4	0.9609
9	143.8	1.493	155.3	2.571	176	3.5
11	156.3	5.405	163.2	5.37	170.7	5.398
13	153.3	3.528	156.2	1.127	166.8	1.217
15	151.2	0.4933	157.3	2.551	167.2	2.551
18	150	0.6506	158	5.014	164.9	4.951
20	148.4	1.976	155.6	3.602	165.6	3.4
22	145.3	2.136	149.2	1.976	158.5*	0.8386
26	150	2.536	154.5	2.248	168.1	2.265
29	147.2	1.361	159.4	2.6	166.9	4.327
34	143.9	1.861	158.8	0.4583	165.7	2.914
39	148.4	1.701	162.9	1.3	168.1	2.128
43	151.9	2.464	168.9	4.081	167.9	2.957

Table 7. Z-Average mean (three measurements) and standard deviation (SD) of sucrose stearate stabilized dispersion during time stability investigation.

	SS δ = 98		**SS δ = 85**		**SS δ = 73**	
Days	Mean	SD	Mean	SD	Mean	SD
1	145.5	2.452	149.4	3.424	171.1	2.771
4	136.8	5.107	139.3	4.188	123	3.1
7	144.4	2.007	131.4	1.1	159.2	1.6
9	145	1.358	122.2*	1.931	174	1.85
11	144.8	2.663	135.6	6.72	197.3	1.127
13	143.8	4.912	162	4.491	261.3	8.915
15	141.5	3.02	203	6.292	277.1	1.973
18	166.2	1.609	257.5	4.576	352.4	17.68
20	184.2	1.762	247.1	5.501		
22	197.9	0.9452	262.3	4.104		
26	210.2	2.501	570.1	8.858		
29	209	0.9165	650.4	5.2		
34	202.7	0.2646				
39	236	3.066				
43	237.1	2.892				

7 References

[1] D. Small, “A classification of biologic lipids based upon their interaction in aqueous systems,” *Journal of the American Oil Chemists' Society,* vol. 45, no. 3, pp. 108-128, 1968.

[2] J. R. Bruckner, “A first example of a lyotropic smectic C* analog phase,” Springer International Publishing Switzerland, Stuttgart, 2016.

[3] C. Fong, T. le and C. Drummond, “Lyotropic liquid crystal engineering–ordered nanostructured small molecule amphiphile self-assembly materials by design,” *Chemical society reviews,* vol. 41, pp. 1297-1322, 2012.

[4] A. Iglic, C. Kulkarni and M. Rappolt, “Steric Stabilizers for Cubic Phase Lyotropic Liquid Crystal Nanodispersions (cubosomes),” in *Advances in Planar Lipid Bilayers and Liposomes*, Academic Press, 2015, pp. 131-176.

[5] C. Kulkarni, W. Watcher, G. Iglesias-Salto, S. Engelskirchen and S. Ahualli, “Monoolein: a magic lipid?,” *Physical Chemistry Chemical Physics,* no. 13, pp. 3004-3021, 2011.

[6] A. Yaghmur, J. Østergaard, S. Larsen, H. Jensen, C. Larsen and M. Rappolt, “Drug formulations based on self-assembled liquid crystalline nanostructures,” in *Liposomes, Lipid Bilayers and Model Membranes*, CRC Press , 2014, p. 341–360.

[7] I. Amar-Yuli, D. Libster, A. Aserin and N. Garti, “Solubilization of food bioactives within lyotropic liquid crystalline mesophases,” *Current opinion in colloid & interface science,* vol. 14, pp. 21-32, 2009.

[8] Z. Karami and H. M, “Cubosomes: remarkable drug delivery potential,” *Drug Discovery Today,* vol. 21, no. 5, 2016.

[9] L. van't Hag, S. Gras, C. Conn and C. Drummond, “Lyotropic liquid crystal engineering moving beyond binary compositional space - ordered nanostractured amphiphile self-assembly materials by design,” *Chemical society reviews,* 2017.

[10] Univeritat Heidelberg, “Theoretical physics: physics of complex biosystems,” 13 11 2000. [Online]. Available: http://www.thphys.uni-heidelberg.de/~biophys/html/BicontinuousPhases/index.html. [Accessed 12 07 2017].

[11] C. V. Kulkarni, T. Y. Tang, A. M. Seddon, J. M. Seddon, O. Ces and R. H. Templer, “Engineering bicontinuous cubic structures at the nanoscale-the role of chain splay,” *Soft Matter,* vol. 6, pp. 3191-3194, 2010.

[12] M. E. Leser, L. Sagalowicz, M. Michael and H. J. Watzke, “Self-assembly of polar food lipids,” *Advances in Colloid and Interface Science,* vol. 123, pp. 125-136, 2006.

[13] A. Li, “Effects of an omega 3 fatty acid on the phase behavior of self-assembled monoglycerides studied by small angle X-ray scattering,” University of Leeds, Leeds, 2016.

[14] A. Sadeghpour, D. Sanver and M. Rappolt, “Interactions of Flavonoids With Lipidic Mesophases,” in *Advances in Biomembranes and Lipid Self-Assembly* , Elsevier B.V., 2017, pp. 95-123.

[15] A. Sadeghpour and M. Rappolt, “Lyotropic liquid crystalline phases for the formulation of future functional foods,” *Journal of nutritional health and food engineering,* vol. 5, no. 1, 2016.

[16] N. Garti, A. Spernath, A. Aserin and R. Lutz, “Nano-sized self-assemblies of nonionic surfactants as solubilization reservoirs and microreactors for food systems,” *Soft matter,* vol. 1, pp. 206-218, 2005.

[17] L. Sagalowicz, C. Moccand, T. Davidek, R. Ghanbari, I. Martiel, R. Negrini, R. Mezzenga, M. Leser, I. Blank and M. Michel, “Lipid self-assembled structures for reactivity control in food,” *Philosophical transaction of the royal society,* vol. 374, 2015.

[18] N. Zeng, X. Gao, Q. Hu, Q. Song, H. Xia, Z. Liu, G. Gu, M. Jiang, Z. Pang, H. Chen, J. Chen and L. Fang, “Lipid-based liquid crystalline nanoparticles as oral drug delivery

vehicles for poorly water-soluble drugs: cellular interaction and in vivo absorption," *International Journal of nanomedicine,* vol. 7, pp. 3703-3718, 2012.

[19] M. Aragón, P. Lavela, B. León, C. Pérez-Vicente, J. Tirado and C. Vidal-Abarca, "On the use of the reverse micelles synthesis of nanomaterials for lithium-ion batteries," *Journal of solid state electrochemistry,* vol. 14, pp. 1749-1753, 2010.

[20] I. Blank, T. Davidek, S. Devaud, L. Sagalowicz, M. Leser and M. Michel, "Formation of 4-hydroxy-5-methyl-3(2H)-furanone (norfuraneol) in structured fluids," *Developments in food science,* vol. 43, pp. 347-350, 2006.

[21] S. Vauthey, C. Milo, P. Frossard, N. Garti, M. Leser and H. Watzke, "Structured fluids as microreactors for flavor formation by the maillard reaction," *Journal of agriculture and food chemistry,* vol. 48, pp. 4808-4816, 2000.

[22] L. Sek, B. Boyd, W. Charman and C. Porter, "Examination of the impact of a range of Pluronic surfactants on the in-vitro solubilisation behaviour and oral bioavailabilty of lipidic formulations of atovaquone," *Journal of pharmacy and pharmacology,* vol. 58, pp. 809-820, 2006.

[23] K. Nagy, B. Lobo, M. Courtet-Compondu, S. Braga-Lagache, L. Ramos, V. Puig-Divi, F. Azpiroz, J. Malagelada, M. Beaumont, J. Moulin, S. Acquistapace, L. Sagalowicz, M. Kussmann, J. Santos, B. Holst and G. Williamson, "Vitamin E and vitamin E acetate absorption from self-assembly systems under pancreas insufficiency conditions," *Chimia,* vol. 68, no. 3, 2014.

[24] B. J. Boyd, S. Khoob, D. V. Whittaker, G. Davey and C. J. H. Porter, "A lipid-based liquid crystalline matrix that provides sustained release and enhanced oral bioavailability for a model poorly water soluble drug in rats," *International Journal of Pharmaceutics,* vol. 340, pp. 52-60, 2007.

[25] R. Negrini and R. Mezzenga, "pH-responsive lyotropic liquid crystals for controlled drug delivery," *Langmuir,* vol. 27, pp. 5296-5303, 2011.

[26] A. Linkeviciute, A. Misiunas, E. Naujalis and J. Barauskas, “Preparation and characterization of quercetin-loaded lipid piquid crystalline systems,” *Colloids and surfaces B: Biointerfaces,* vol. 128, pp. 296-303, 2015.

[27] W. Sun, J. J. Vallooran, A. Zabara and R. Mezzenga, “Controlling enzymatic activity and kinetics in swollen mesophases by physical nano-confinement,” *Nanoscale,* vol. 6, pp. 6853-6859, 2014.

[28] A. Tyler, M. Barringa, E. Parsons, N. McCarthy, O. Ces, R. Law, J. Seddon and N. Brooks, “Electrostatic swelling of bicontinuous cub lipid phases,” *Soft matter,* vol. 11, pp. 3279-3286, 2015.

[29] L. Sagalowicz and M. Leser, “Delivery systems for liquid food products,” *Current opinion in colloid and interface science,* vol. 15, pp. 61-72, 2010.

[30] S. Serieye, F. Meducine, I. Milosevic, L. Fu and S. Guillot, “Interface tuning and stabilization of monoglyceride mesophase dispersions: food emulsifiers and mixtures efficiency,” *Journal of colloid and interface science,* pp. 26-34, 2017.

[31] S. Guillot, S. Salentinig, A. Chemelli, L. Sagalowicz, M. E. Leser and O. Glatter, “Influence of the stabilizer concentration on the internal liquid crystalline order and the size of oil-loaded monolinolein-based dispersion,” *Langmuir,* vol. 26, no. 9, pp. 6222-9, 2009.

[32] C. Ruxton, S. Reed, M. Simpson and K. Millington, “The health benefits of omega-3 polyunsaturated fatty acids: a review of the evidence,” *Journal of human nutrition and dietetics,* vol. 17, pp. 449-459, 2004.

[33] J. Schuchardt and A. Hahn, “Bioavailability of long-chain omega-3 fatty acids,” *Prostaglandins, Leukotrienes and essential fatty acids,* vol. 89, pp. 1-8, 2013.

[34] M. Bouwens, O. van de Rest, N. Dellschaft, M. Bromhaar, L. C. de Groot, J. Geleijnse, M. Muller and L. Afman, “Fish-oil supplementation induces antiinflammatory gene expression profiles in human blood mononuclear cells,” *The American journal of clinical nutrition,* vol. 90, pp. 415-424, 2009.

[35] S. Lorente-Cebrián, A. Costa, S. Navas-Carretero, M. Zabala, J. Martínez and M. Moreno-Aliaga, “Role of omega-3 fatty acids in obesity, metabolic syndrome, and cardiovascular diseases: a review of the evidence,” *Journal of physiology and biochemistry,* vol. 69, no. 3, pp. 633-651, 2013.

[36] EFSA Panel on Dietetic Products, Nutrition, and Allergies, “Scientific opinion on dietary reference values for fats, including saturated fatty acids, polyunsaturated fatty acids, monounsaturated fatty acids, trans fatty acids, and cholesterol,” *EFSA journal,* vol. 8, no. 3, 2010.

[37] A. Hill, J. Buckley, K. Murphy and P. Howe, “Combining fish-oil supplements with regular aerobic exercise improves body composition and cardiovascular disease risk factors,” *American journal of clinical nutrition,* vol. 85, pp. 1267-1274, 2007.

[38] D. Swanson, R. Block and S. Mousa, “Omega-3 fatty acids EPA and DHA: health benefits throughout life,” *Advances in nutrition,* vol. 3, pp. 1-7, 2012.

[39] M. Judge, O. Harel and C. Lammi-Keefe, “Maternal consumption of a docosahexaenoic acid– containing functional food during pregnancy: benefit for infant performance on problem-solving but not on recognition memory tasks atage 9 mo,” *The Akmerican journal of clinical nutrition,* vol. 85, pp. 1572-1577, 2007.

[40] J. Dunstan, K. Simmer, G. Dixon and S. Prescott, “Cognitive assessment of children at age 2 1/2 years after maternal fish oil supplementation in pregnancy: a randomised controlled trial,” *Archives of disease in childhood-fetal and neonatal,* vol. 93, 2008.

[41] I. Sioen, L. van Lieshout, A. Eilander, M. Fleith, S. Lohner, A. Szommer, C. Petisca, S. Eussen, S. Forsyth, P. Calder, C. Campoy and R. Mensink, “Systematic review on N-3 and N-6 polyunsaturated fatty acid intake in European countries in light of the current recommendations – Focus on specific population gruops,” *Annals of nutrition and metabolism,* vol. 70, pp. 39-50, 2017.

[42] M. Michael, H. Watzke, L. Sagalowicz, E. Kolodziejczyk and M. E. Leser, “Self-assembly in food - A new way to make nutritious products,” in *Food colloids: self-assembly and material science*, Cambridge, RSC Pub, 2007.

[43] S. Salentinig, S. Phan, J. Khan, A. Hawley and B. Boyd, “Formation of highly organized nanostructures during the digestion of milk,” *American chemical society,* vol. 7, no. 12, pp. 10904-10911, 2013.

[44] M. Buttet, V. Traynard, T. Tran, P. Besnard, H. Poirier and I. Niot, “From fatty-acid sensing to chylomicrons synthesis: role of intestinal lipid-binding proteins,” *Biochimie,* vol. 96, pp. 37-47, 2014.

[45] C. Porter, N. Trevaskis and W. Charman, “Lipids and lipid-based formulations: optimizing the oral bioavailability of lipophilic drugs,” *Nature reviews- Drug discovery,* vol. 6, p. 231, 2007.

[46] X. Jin, Z. Z., S. Li, E. Sun, X. Tan, J. Song and X. Jia, “A nanostructured liquid crystalline formulation of 20(S)-protopanaxadiol with improved oral absorption,” *Fitoterapia,* vol. 84, pp. 64-71, 2013.

[47] S. Salentinig, L. Sagalowicz, M. Leser, C. Tedeschi and O. Glatter, “Transitions in the internal structure of lipid dropltes during fat digestion,” *Soft matter,* vol. 7, pp. 650-661, 2011.

[48] M. Lindstrom, H. Ljusberg-Wahren, K. Larsson and B. Borgstrom, “Aqueous lipid phases of relevance to intestinal fat digestion and adsorption,” *Lipids,* vol. 16, no. 10, 1981.

[49] I. Amar-Yuli, A. Aserin and N. Garti, “Solubilization of nutraceuticals into reverse hexagonal mesophases,” *Journal of physical chemestry B,* vol. 112, pp. 10171-10180, 2008.

[50] M. Baker and H. Cohen, “An explanation of Miller indices,” 2004.

[51] M. Rappolt, “The biologically relevant lipid mesophases as ”seen” by X-rays,” in *Advances in planar lipid bilayers and liposomes (vol. 5)*, Amsterdam, Elsevier Inc., 2006, pp. 253-283.

[52] T. Li, A. Senesi and B. Lee, “Small angle X-ray scattering for nanoparticle research,” *American chemical society,* vol. 116, pp. 11128-11180, 2016.

[53] H.-J. Bautsch, J. Bohm and I. Kleber, “Kristallstrukturlehre und kristallmorphologie,” in *Einführung in die Kristallographie*, Verlag Technik, 1956.

[54] Malvern, “ATA scientific instruments,” [Online]. Available: http://149.171.168.221/partcat/wp-content/uploads/Malvern-Zetasizer-LS.pdf.

[55] Malvern, Zetasizer nano series-user manual, United Kingdom: Malvern Instruments Ltd., 2013.

[56] MOLBASE, “MOLBASE: Chemical Dictionary,” [Online]. Available: http://www.molbase.com/en/2277-28-3-moldata-1547452.html. [Accessed 31 08 2017].

[57] A. Boentaran, “Influence of omega-3 composition and external temperature on the phase behaviour of monolinolein nanostructures: an investigation,” University of Leeds, Leeds, 2017.

[58] M. Pouzot, R. Mezzenga, M. Leser, L. Sagalowicz, S. Guillot and O. Glatter, “Structural and rheological investigation of Fd3m inverse micellar cubic phases,” *Langmuir,* vol. 19, no. 23, pp. 9618-9628, 2007.

[59] S. Guillot, C. Moitzi, S. Salentinig, L. Sagalowicz, M. E. Leser and O. Glatter, “Direct and indirect thermal transition from hexosomes to emulsified micro-emulions in oil-loaded monoglyceride-based particles,” *Colloids and Surfaces,* no. 291, pp. 78-84, 2006.

[60] B. J. Boyd, S. Khoo, D. Whittaker, G. Davey and C. Porter, “A lipid-based liquid crystalline matrix that provides sustained release and enhanced oral

bioavailability for a model poorly water soluble drug in rats," *International journal of pharmaceutics,* vol. 340, pp. 52-60, 2007.